Structures, Dynamics, and Biological Activities of 15 Cyclic Hexapeptide Analogs of the α-Amylase Inhibitor Tendamistat (HOE 467) in Solution

Hans Matter† and Horst Kessler*

Contribution from the Institut für Organische Chemie und Biochemie, Technische Universität München, Lichtenbergstrasse 4, D-85747 Garching, Germany

Received November 10, 1994®

Abstract: The design, synthesis, and conformational analysis of a series of 15 cyclic hexapeptides as analogs of the active sequence of the α-amylase inhibitor protein Tendamistat (HOE 467) Ser^{17}-Trp^{18}-Arg^{19}-Tyr^{20} are described. A template-oriented peptide design strategy was used to expose this tetrapeptide motif to different conformational environments. Conformational analysis was carried out for each peptide in DMSO-d_6 solution by means of NMR spectroscopy. For structure determination, restrained molecular dynamics (MD) simulations *in vacuo* and in DMSO based on experimentally derived distance and torsion constraints were performed. For eight peptides, experimental data were found to be inconsistent unless multiple fast interconverting backbone conformers were taken into account. For these peptides the NMR observables can only be described by averaging over conformational ensembles containing at least two major backbone conformations. All other compounds can be described by a single backbone conformation. Some general rules for rigidification of peptide backbone conformations can be verified by analyzing different peptide structures. It could further be shown that the use of backbone templates forces the tetrapeptide sequence to adopt its native conformation, as found in solution and crystal structures of Tendamistat. Significant biological activity as α-amylase inhibitors could be measured for these peptides. However, the suggested active tetrapeptide sequence alone is not responsible for the strong binding between Tendamistat and α-amylase, which is supported by the inspection of the preliminary solid-state structure of the Tendamistat/α-amylase complex.

1. Introduction

Tendamistat (HOE 467), an extracellular protein containing 74 amino acids, shows significant biological activity as an α-amylase inhibitor.[1,2] α-Amylase [α(1→4)-glucan-4-glucanohydrolase, EC 3.2.1.1.] is an important enzyme in the process of carbohydrate degradation.[3] It catalyzes the hydrolysis of α-(1→4) glycosidic linkages in starch, glycogen, or synthetic oligosaccharides. Inhibitors of this enzyme are of major pharmaceutical interest due to their ability to regulate the degradation of starch in treatment of *diabetes mellitus*.[4]

A pseudo-irreversible complex between Tendamistat and α-amylase (496 amino acids for porcine pancreas α-amylase) with a K_I value of 2×10^{-10} M is formed. Due to its resistance against most hydrolytic enzymes, Tendamistat would be orally applicable for *diabetes mellitus* treatment. However, its immunogeneity recently found prevents Tendamistat from being ideally suited for this purpose.[5] This leads to an interest in smaller cyclic peptides containing the active sequence Ser^{17}-Trp^{18}-Arg^{19}-Tyr^{20} of Tendamistat in its native geometrical arrangement but not having these unwanted side effects.

The known solution[6] and crystal structure[7] of this amylase inhibitor initiated our studies to mimic the conformation of the active tetrapeptide sequence—found at the top of the first hairpin loop in Tendamistat in a reverse turn arrangement—by cyclic peptides. Cyclic peptides can serve either as model compounds to study conformational preferences or as templates to force some amino acid sequences into well-defined conformations.[8]

Three main questions are addressed by these studies:

(1) Is it possible to include a tetrapeptide sequence in a cyclic hexapeptide template so that the spatial arrangements of these residues in their native "biologically active" conformation are maintained?

(2) Which forces lead the active sequence in Tendamistat to adopt its spatial reverse turn arrangement?

(3) Does a geometrical match of certain key features in solution between cyclic peptides and the first loop in Tendamistat induce biological activity, or are there more residues responsible for the tight binding of Tendamistat to the α-amylase?

Therefore the importance of the proposed tetrapeptide sequence for any inhibitory effect in Tendamistat was explored. Here we describe the design, synthesis, and conformational analyses of 15 cyclic hexapeptide analogs including this active

* To whom correspondence should be addressed.
† Current address: TRIPOS Associates, Martin-Kollar-Str. 15, D-81829 München, Germany.
® Abstract published in *Advance ACS Abstracts,* March 1, 1995.

(1) Aschauer, H.; Vértesy, L.; Braunitzer, G. *Z. Physiol. Chem.* **1981**, *362*, 465−467.
(2) Vértesy, L.; Oeding, V.; Bender, R.; Zepf, K.; Nesemann, G. *Eur. J. Biochem.* **1984**, *141*, 505−512.
(3) (a) Kluh, I. *FEBS Lett.* **1981**, *136*, 231−234. (b) Nakajima, R.; Imanaka, T.; Aiba, S. *Appl. Microbiol. Biotechnol.* **1986**, *23*, 355−360. (c) Pasero, L.; Mazzei-Pierron, Y.; Abadie, B.; Chicheportiche, Y.; Marchis-Mouren, G. *Biochim. Biophys. Acta* **1986**, *869*, 147−157.
(4) (a) Puls, W.; Keup, U. *Diabetologia* **1973**, *7*, 97. (b) Truscheit, E.; Frommer, W.; Junge, B.; Müller, L.; Schmidt, D. D.; Wingender, W. *Angew. Chem.* **1981**, *93*, 738−755.
(5) Vertésy, L.; Bender, R.; Engels, J. Personal communication.
(6) (a) Kline, A. D.; Wüthrich, K. *J. Mol. Biol.* **1985**, *183*, 503−507. (b) Kline, A. D.; Braun, W.; Wüthrich, K. *J. Mol. Biol.* **1986**, *189*, 377−382. (c) Qiwen, W.; Kline, A. D.; Wüthrich, K. *Biochemistry* **1987**, *26*, 6488−6493. (d) Billeter, M.; Schaumann, T.; Braun, W., Huber, R.; Wüthrich, K. *Biopolymers* **1990**, *29*, 695−706.
(7) (a) Pflugrath, J. W.; Wiegand, G.; Huber, R.; Vértesy, L. *J. Mol. Biol.* **1986**, *189*, 383−386. (b) Braun, W.; Epp, O.; Wüthrich, K.; Huber, R. *J. Mol. Biol.* **1989**, *206*, 669−676. (c) Brünger, A. T.; Kuriyan, J.; Karplus, M. *Science* **1987**, *235*, 458−460. (d) Billeter, M.; Kline, A. D.; Braun, W.; Huber, R.; Wüthrich, K. *J. Mol. Biol.* **1989**, *206*, 677−687.
(8) Kessler, H. *Angew. Chem.* **1982**, *94*, 509−520.

0002-7863/95/1517-3347$09.00/0

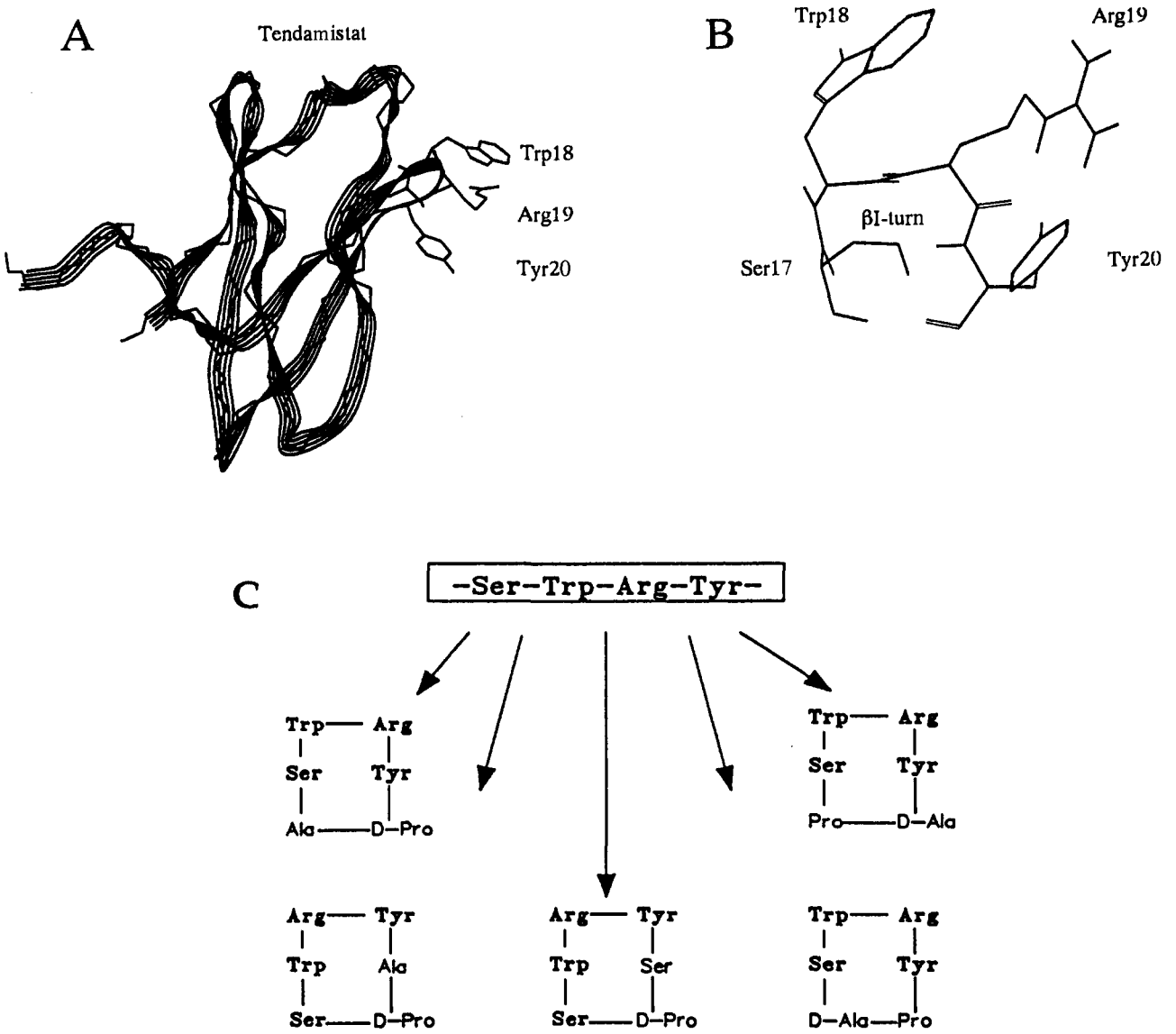

Figure 1. Peptide design using the solution structure of the α-amylase inhibitor Tendamistat as determined by NMR spectroscopy. (A) Representative *distance geometry* structure for Tendamistat obtained using the program DISMAN (Brookhaven entry 3ait).[6b] The protein backbone is indicated by a ribbon display, only side chains for the active sequence at the top of the first loop are shown. (B) Tendamistat tetrapeptide sequence Ser^{17}-Trp^{18}-Arg^{19}-Tyr^{20} in its native type-I turn conformation,[6b] which is responsible for the tight binding to α-amylase. This sequence was derived from comparisons with homolog proteins.[2] (C) Five cyclic hexapeptide templates to constrain the tetrapeptide sequence. The tetrapeptide is exposed in different conformational environments within each template.

sequence. The structure determinations were carried out using a well-explored combination of NMR spectroscopy and MD simulations utilizing experimentally derived constraints for calculations *in vacuo* and in DMSO solution. The analysis of the structures and their match to the target conformation of the protein will be described here.

2. Design of Cyclic Peptides

The geometrical similarity of Tendamistat structures determined in different environments was used as an indicator for related structural preferences in the Tendamistat/amylase complex. In both environments (entries 1HOE (X-ray structure) or 3AIT/4AIT (NMR structures) in the Brookhaven database), the active sequence from sequence comparisons of different homolog amylase inhibitors,[2] forms a βI-turn[9] with Trp^{18} and Arg^{19} in positions i and $i + 1$, respectively, which is additionally stabilized by two hydrogen bonds: a standard 4→1 backbone hydrogen bond between Ser^{17}CO and Tyr^{20}NH and an additional main chain–side chain hydrogen bond from $Ser^{17}O_\gamma$ to $Arg^{19}N_\alpha H$. The latter one forces the orientation of the central $(i + 1) - (i + 2)$ amide bond to adopt the βI-conformation (cf. Figure 1).

The design procedure is illustrated in Figure 1: structural constraints are imposed by cyclization on the active sequence. Different arrangements of two fused β-turns are used to force the tetrapeptide fragment Ser-Trp-Arg-Tyr into different β-turn conformations while maintaining the cyclic hexapeptide template. Modifications of the position of a D-amino acid relative to the tetrapeptide sequence result in a "shift" of this sequence: now different amino acids adopt the positions i to $i + 3$ of a generalized reverse turn structure, respectively.

Furthermore, the substitution of Arg^{19} against two other basic amino acids (Lys or Orn) is used to study the influence of the basic guanidino-functional group on enzyme binding, compared to the less basic amino groups in the substituted amino acids. Different spatial arrangements of the cyclization dipeptide fragment should be used for correlation of this effect with biological activity.

(9) (a) Rose, G. D.; Gierasch, L. M.; Smith, J. A. *Adv. Protein Chem.* **1985**, *37*, 1–109. (b) Smith, J. A.; Pease, L. G. *CRC Crit. Rev. Biochem.* **1980**, 315–399.

Chart 1. Amino Acid Sequences of All 15 Cyclic Hexapeptides with Protecting Groups

C1	cyclo(-D-Pro^1-Ala^2-Ser^3(Bzl)-Trp^4-Lys^5(Z)-Tyr^6-)
C2	cyclo(-D-Pro^1-Ala^2-Ser^3(Bzl)-Trp^4-Orn^5(Z)-Tyr^6-)
C3	cyclo(-D-Pro^1-Ala^2-Ser^3-Trp^4-Arg^5(NO$_2$)-Tyr^6-)
C4	cyclo(-D-Pro^1-Ser^2(Bzl)-Trp^3-Lys^4(Z)-Tyr^5-Ala^6-)
C5	cyclo(-D-Pro^1-Ser^2(Bzl)-Trp^3-Orn^4(Z)-Tyr^5-Ala^6-)
C6	cyclo(-D-Pro^1-Ser^2-Trp^3-Arg^4(NO$_2$)-Tyr^5-Ala^6-)
C7	cyclo(-D-Pro^1-Ser^2-Trp^3-Lys^4(Z)-Tyr^5-Ser^6(Bzl)-)
C8	cyclo(-D-Pro^1-Ser^2(Bzl)-Trp^3-Orn^4(Z)-Tyr^5-Ser^6(Bzl)-)
C9	cyclo(-D-Pro^1-Ser^2-Trp^3-Arg^4(NO$_2$)-Tyr^5-Ser^6-)
C10	cyclo(-Pro^1-D-Ala^2-Ser^3-Trp^4-Lys^5(Z)-Tyr^6-)
C11	cyclo(-Pro^1-D-Ala^2-Ser^3-Trp^4-Orn^5(Z)-Tyr^6-)
C12	cyclo(-Pro^1-D-Ala^2-Ser^3-Trp^4-Arg^5(NO$_2$)-Tyr^6-)
C13	cyclo(-D-Ala^1-Pro^2-Ser^3(Bzl)-Trp^4-Lys^5(Z)-Tyr^6-)
C14	cyclo(-D-Ala^1-Pro^2-Ser^3(Bzl)-Trp^4-Orn^5(Z)-Tyr^6-)
C15	cyclo(-D-Ala^1-Pro^2-Ser^3-Trp^4-Arg^5(NO$_2$)-Tyr^6-)

From the utilization of these different design strategies, five different classes of cyclic hexapeptides result, differing in their backbone geometries, with three different peptides in each class (Arg, Lys, or Orn as the "basic" amino acid). These 15 peptides were synthesized, and their conformations were analyzed (cf. Chart 1).

In parallel studies by Etzkorn et al.,[10] the program CAVEAT[11] was used to design new molecular frameworks to fix the functional groups of the amino acid side chains in their proper positions. A small molecule, which imitates the "active loop" of a macromolecular ligand with its spatial and electronical properties may mimic its binding properties as well. With this approach a rigid template is designed. The templates, which would hold the Cα−Cβ bonds of the amino acid side chains in a relative orientation similar to that found in Tendamistat, are mainly based on cyclic peptide models, leading again to cyclic hexapeptides as mimics of the structure of Tendamistat.[10]

3. Experimental Methods

3.1. Synthesis. All 10 cyclic peptides without Arg were synthesized by following Merrifield's solid phase technique[12] using the Boc protective group strategy. The first amino acids, Boc-Ser(Bzl)-OH[13] and Boc-Ser-OH, were esterified to the chloromethylated polystyrene by the Cesium salt method.[14] Chain elongation was carried out by following the Boc-TFA scheme; the peptides were cleaved from the resin with hydrazine. The N-terminal Boc protective groups were removed with TFA, and cyclization was achieved via the azide method.[15] The crude products were purified by Sephadex gel filtration and/or flash chromatography on silica gel and finally by HPLC. All protecting groups were cleaved by hydrogenation in dry methanol (Ser(Bzl) deprotections require a mixture of methanol and acetic acid) on a Pd/C catalyst. For some peptides the cleavage of the protecting groups was carried out using liquid HF. Finally the deprotected peptides were purified by reversed-phase HPLC.

Chart 2. Solution-Phase Syntheses of C3, C6, C9, C12, and C15

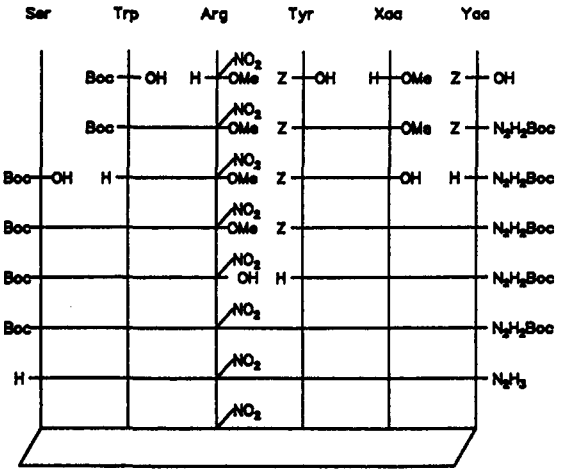

[a] Xaa, Yaa = C6: Ala, D-Pro; C9: Ser, D-Pro; C12: Pro, D-Ala; C15: D-Ala, Pro.

All peptide containing Arg (C3, C6, C9, C12, and C15) were synthesized by peptide synthesis in solution by following a convergent strategy and a final 3 + 3 fragment condensation, as shown in Chart 2, to build the linear hexapeptide precursors. The fragment Boc-Ser-Trp-Arg(NO$_2$)-OH, which is available in good yields, was used as the N-terminal building block for all five different peptides. All five different C-terminal peptides are also available in good overall yields. After final purifications of the linear precursors, the *N'*-Boc-hydrazides and the N-terminal Boc protecting groups were removed in one step and subsequent cyclization was achieved via the azide method. Purifications of crude products and deprotections of blocking groups were done as described above.

3.2. NMR Measurements. A variety of homo- and heteronuclear 2D-NMR techniques provided ^{1}H and ^{13}C assignments for all peptides. Homonuclear spin systems were identified using TOCSY[16] and DQF-COSY[17] experiments. The sequential assignment of all spin systems identified was possible using NOESY[18] or ROESY spectra[19] and was confirmed via the analysis of heteronuclear long-range correlations (selective HMBCS-270[20,21]). Via HMQC[22] and HMQC-TOCSY spectra,[23] the assignment of the ^{13}C resonances was completed.

Quantitative information on interproton distances for the structure determination was obtained from analyzing NOESY

(10) Etzkorn, F. A.; Guo, T.; Lipton, M. A.; Goldberg, S. D.; Bartlett, P. A. *J. Am. Chem. Soc.*, in press.

(11) (a) Bartlett, P. A.; Shea, G. T.; Telfer, S. J.; Waterman, S. *Molecular Recognition: Chemical and Biochemical Problems*; Roberts, S. M., Ed.; Royal Society of Chemistry: Exeter, U.K., 1990. (b) Lauri, G.; Bartlett, P. A. *J. Comput.-Aided Mol. Des.* **1994**, *8*, 51−66.

(12) (a) Merrifield, R. B. *J. Am. Chem. Soc.* **1963**, *85*, 2149−2154. (b) Stewart, J.; Young, J. *Solid Phase Peptide Synthesis*; Freeman & Co.: San Francisco, CA, 1969. (c) Barany, G.; Kneib-Cordonnier, N.; Mullen, D. G. *Int. J. Pept. Protein Res.* **1987**, *30*, 705−739.

(13) Bodanszky, M.; Bodanszky, A. *The Practice of Peptide Synthesis*; Springer: Berlin, 1984.

(14) Gisin, B. F. *Helv. Chem. Acta* **1973**, *56*, 1476−1482.

(15) Klausner, Y. S.; Bodanszky, M. *Synthesis* **1974**, 549−559.

(16) (a) Braunschweiler, L.; Ernst, R. R. *J. Magn. Reson.* **1983**, *53*, 521−528. (b) Bax, A.; Byrd, R. A.; Aszalos, A. *J. Am. Chem. Soc.* **1984**, *106*, 7632−7633. (c) Bax, A.; Davis, D. G. *J. Magn. Reson.* **1985**, *65*, 355−360.

(17) (a) Piantini, U.; Sørensen, O. W.; Ernst, R. R. *J. Am. Chem. Soc.* **1982**, *104*, 6800−6801. (b) Rance, M.; Sørensen, O. W.; Bodenhausen, G.; Wagner, G.; Ernst, R. R.; Wüthrich, K. *Biochem. Biophys. Res. Commun.* **1983**, *117*, 458−479.

(18) Jeener, J.; Meier, B. H.; Bachmann, P.; Ernst, R. R. *J. Chem Phys.* **1979**, *71*, 4546−4553.

(19) (a) Bothner-By, A. A.; Stephens, R. L.; Lee, J.; Warren, C. D.; Jeanloz, R. W. *J. Am. Chem. Soc.* **1984**, *106*, 811−813. (b) Bax, A.; Davis, D. G. *J. Magn. Reson.* **1985**, *63*, 207−213. (c) Kessler, H.; Griesinger, C.; Kerssebaum, R.; Wagner, K.; Ernst, R. R. *J. Am. Chem. Soc.* **1987**, *109*, 607−609.

(20) Bax, A.; Summers, M. F. *J. Am. Chem. Soc.* **1986**, *108*, 2093−2094.

(21) (a) Bermel, W.; Wagner, K.; Griesinger, C. *J. Magn. Reson.* **1989**, *83*, 223−232. (b) Emsley, L.; Bodenhausen, G. *J. Magn. Reson.* **1989**, *82*, 211−221. (c) Kessler, H.; Schmieder, P.; Köck, M.; Kurz, M. *J. Magn. Reson.* **1990**, *88*, 615−618.

(22) (a) Müller, L. *J. Am. Chem. Soc.* **1979**, *101*, 4481−4484. (b) Bax, A.; Griffey, R. H.; Hawkins, L. B. *J. Magn. Reson.* **1983**, *55*, 301−315.

(23) Lerner, A.; Bax, A. *J. Magn. Reson.* **1986**, *69*, 375−380.

spectra[18] with 150 ms mixing times without zero-quantum suppression or ROESY spectra[19] with 180 ms mixing times. If ROESY spectra were analyzed, it was checked that no NOE effects occurred at the field strength chosen. This was exclusively the case for the 250 MHz proton resonance frequency. Peak volumes were integrated on both sides of the diagonal and averaged. For a correct conversion of measured ROESY integral volumes into geometric parameters, the offset effect was taken into account.[24] All distance calculations were carried out using the isolated two-spin approximation (ISPA).[25]

The experimental data set with interproton distances including constraints for diastereotopically assigned protons was used in all 15 cases for subsequent molecular dynamics (MD) structure determinations and refinement. Additionally, selected backbone dihedral angles calculated from homo- and heteronuclear coupling constants were used to check the conformational model during the MD refinement. Temperature coefficients of amide proton chemical shifts and populations of different side chain χ_1 rotamers were determined and analyzed by following previously described methods (see, for example, ref 26). To get more experimental insight in the dynamics of these peptides, proton $T_{1\varrho}$ measurements[27] of amide protons were carried out for selected peptides (C2, C2e, C4, C7, C10, and C13) as a function of different spin-lock fields B_1 at 500 MHz proton resonance frequency.

3.3. Molecular Dynamics (MD) Simulation. Molecular dynamics (MD) simulations were performed for all 15 peptides (without protecting groups) using their experimental data as additional restraints using the program package GROMOS (Biomos)[28] on Silicon Graphics 4D/240SX and 4D/70GTB computers. The kinetic energy was included by coupling the system to a thermal bath.[29] Due to the application of the SHAKE algorithm, the step size for the integration of Newton's equation (*Verlet* algorithm[30]) was set to 2 fs. Selected side chains were fixed in their dominantly populated conformations. An additional harmonic restraint function was employed for upper and lower distance bounds. The function switches from harmonic to linear when the deviation is greater than 10% of the target distance. For the upper bounds, standard pseudoatom corrections were added, if necessary. Details of the used experimental data are given in the supplementary material.

Manually built random starting structures were energy minimized prior to MD simulations. Standard MD refinement protocols were used for all compounds: during the first picosecond, the system was coupled to a 1000 K temperature bath with a force constant of 4000 kJ mol^{-1} nm^{-2} (K_{dc}) for distance restraints, while in the next 5 ps, the temperature was scaled down to 500 K and finally to 300 K. For the following simulation period of 60 ps at 300 K, K_{dc} was reduced to 1000 kJ mol^{-1} nm^{-2}. After an initial equilibration period of 10 ps, the next 50 ps were used for averaging. For selected peptides (C2, C3, C6, C9, C12, and C15), the averaged and minimized structures from *in vacuo* MD simulations were soaked with DMSO (including periodic boundary conditions) using truncated octahedrons[31] with ca. 200–300 DMSO molecules. After initial relaxation of the system, MD simulations covered a time span of ca. 100 ps: 20 ps for equilibration and ca. 60–80 ps for analysis at 300 K with K_{dc} = 1000 kJ mol^{-1} nm^{-2}.

MD simulations with time-dependent distance constraints (MD^{tNOE}) were carried out for eight peptides (C4–C9, C13, and C14) for which experimental data were not in agreement with a single backbone conformer.[32] A modified term to calculate the penalty energies for distance constraints is included; upper and lower bounds must only be satisfied as a $\langle r^{-3}\rangle^{-1/3}$ weighted time average. The artificial force derived from this penalty energy term is increased gradually for the most violated restraints. This technique allows better sampling of the conformational space while using conflicting distance constraints in the refinement procedure.

4. Results

Because of the observed conformational similarity for some peptides investigated here, they are grouped into five different classes for structure discussion. From previous studies[33] and from results presented here, it could be concluded that some side chain protecting groups (Lys(Z), Orn(Z), and Arg(NO$_2$)) do not influence the overall peptide conformation, while for Ser(Bzl), the sometimes observed influence on peptide backbone conformations is dependent on its position in the peptide sequence.[33] This was carefully checked for all classes of cyclic peptides using members for each group without Ser protecting groups (i.e., C3, C6, C9, C12, and C15; cf. Chart 1), conformational analyses of unprotected vs protected peptides (C2 vs C2e[33]), and NMR chemical shift comparisons for protected vs unprotected peptides. Therefore it is possible for these cases to derive conformations of unprotected peptides from their protected precursors.

4.1. Cyclo(-D-Pro^1-Ala^2-Ser^3-Trp^4-Xaa^5-Tyr^6-) (C1, C2, and C3). The resulting structures of peptides C1 (Xaa = Lys(Z); including Ser(Bzl)) and C3 (Xaa = Arg(NO$_2$)) after averaging over a 40 ps MD simulation *in vacuo* (C1) and 80 ps MD simulation in DMSO solution (C3) are given in Figure 2. The corresponding structures including a complete analysis for peptide C2 (Xaa = Orn(Z); including Ser(Bzl)) in comparison to the deprotected peptide C2e are described elsewhere.[33]

For all three peptides a similar pattern of two intramolecular hydrogen bonds from Tyr^{6}NH to Ser$_3$C=O and from Ser^{3}NH to Tyr^{6}C=O is observed. This corresponds to cyclic structures consisting of two fused β-turns. These peptides show a βII'-turn encompassing D-Pro^1 (i + 1) and Ala^2 (i + 2); the associated hydrogen bonds involving Ser^{3}NH are highly populated during the time scale of the dynamics simulations.

The opposite regions in these peptides show significant differences. While for C1 and C2 with a Ser^3(Bzl) residue, a βII-turn in this moiety is observed with Trp^4 and Lys^5 in positions i + 1 and i + 2, for the deprotected peptide C2e and for C3 with a Ser^3 residue, a βI-turn is found. Both reverse-

(24) Griesinger, C.; Ernst, R. R. *J. Magn. Reson.* **1987**, *75*, 261–271.
(25) Neuhaus, D.; Williamson, M. *The Nuclear Overhauser Effect in Structural and Conformational Analysis*; VCH: Weinheim, Germany, 1989.
(26) Kessler, H.; Matter, H.; Gemmecker, G.; Kottenhahn, M.; Bats, J. W. *J. Am. Chem. Soc.* **1992**, *114*, 4805–4818 and references cited therein.
(27) (a) Kopple, K. D.; Wang, Y. S.; Cheng, A. G.; Bhandary, K. K. *J. Am. Chem. Soc.* **1988**, *110*, 4168–4176. (b) Ikuta, S.; Wang, Y. S. *J. Am. Chem. Soc.* **1990**, *112*, 5901–5906. (c) Wang, Y. S.; Ikuta, S. *Magn. Reson. Chem.* **1989**, *27*, 1134–1141. (d) Wang, Y. S.; Ikuta, S. *J. Am. Chem. Soc.* **1989**, *111*, 243–1248. (e) Kopple, K. D.; Wang, Y. S. *Int. J. Peptide Protein Res.* **1989**, *33*, 82–85.
(28) (a) Aqvist, J.; van Gunsteren, W. F.; Leijonmark, M.; Tapia, O. J. *J. Mol. Biol.* **1985**, *183*, 461–477. (b) van Gunsteren, W. F.; Kaptein, R.; Zuiderweg, E. R. P. *Proceedings of the NATO/CECAM Workshop on Nucleic Acid Conformation and Dynamics*; Olsen, W. K., Ed.; Orsay, 1983; pp 79–92. (c) van Gunsteren, W. F.; Boelens, R.; Kaptein, R.; Scheek, R. M.; Zuiderweg, E. R. P. *Molecular Dynamics and Protein Structure*; Hermans, J., Ed.; Polycrystal Book Service: Western Springs, IL, 1985; pp 92–99. (d) van Gunsteren, W. F.; Berendsen, H. J. C. Groningen Molecular Simulation (GROMOS) Library Manual, *GROMOS user manual*; Biomos B. V.: Nijenborgh 16 NL 9747 AG Groningen; pp 1–229.
(29) Berendsen, H. J. C.; Postma, J. P. M.; van Gunsteren, W. F.; Di Nola, A.; Haak, J. R. *J. Chem. Phys.* **1984**, *81*, 3684–3690.
(30) (a) Ryckaert, J. P.; Cicotti, C.; Berendsen, H. J. C. *J. Comput. Phys.* **1977**, *23*, 327–343. (b) van Gunsteren, W. F.; Berendsen, H. J. C. *Mol. Phys.* **1977**, *34*, 1311–1327.
(31) Adams, D. J. *J. Chem. Phys. Lett.* **1979**, *62*, 329–332.
(32) (a) Torda, A. E.; Scheek, R. M.; van Gunsteren, W. F. *Chem. Phys. Lett.* **1989**, *157*, 289–294. (b) Torda, A. E.; Scheek, R. M.; van Gunsteren, W. F. *J. Mol. Biol.* **1990**, *214*, 223–235.
(33) Matter, H.; Gemmecker, G.; Kessler, H. *Int. J. Pept. Protein Res.*, in press.

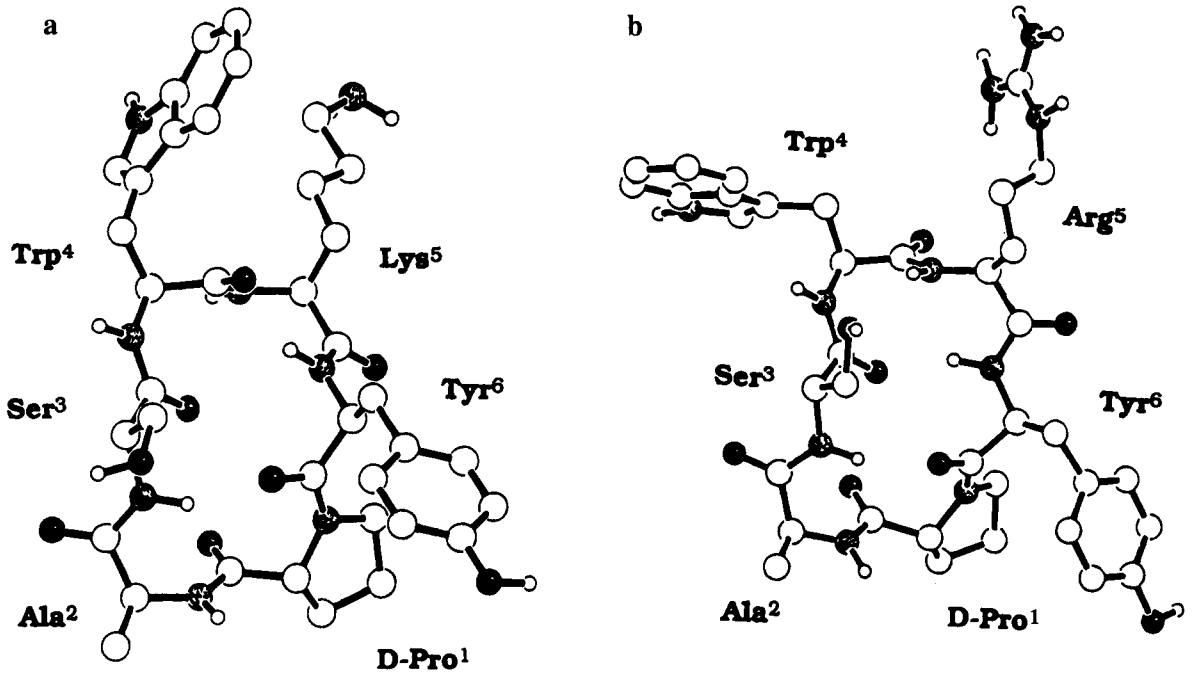

Figure 2. (a) Averaged structure for cyclo(-D-Pro[1]-Ala[2]-Ser[3](Bzl)-Trp[4]-Lys[5](Z)-Tyr[6]-) (C1) from 50 ps restrained MD *in vacuo*. No experimental information is available for the side chain conformations of Ser[3], Trp[4], and Lys[5]. (B) Averaged structure for cyclo(-D-Pro[1]-Ala[2]-Ser[3]-Trp[4]-Arg[5]-(NO_2)-Tyr[6]-) (C3) from 80 ps restrained MD in DMSO. No experimental information is available for the side chain conformations of Ser[3], Trp[4], and Arg[5]. Protecting groups and nonlabile hydrogens are not displayed.

turn motifs are stabilized by main chain hydrogen bonds (Tyr[6]NH to Ser[3]C=O). Both the βI- and βII-turn structures differ with respect to the relative orientation of the central Trp[4] to Orn[5] amide bond compared to the plane defined by all C_α atoms in these peptides. The βI-turn motif is additionally stabilized by a main chain-side chain hydrogen bond; the Ser[3]O_γ is involved in hydrogen bonds to Orn[5]N*H* ($i + 2$) and Tyr[6]N*H* ($i + 3$), forming a bifurcated network in some structures of the analyzed MD trajectories.[32] This hydrogen bond motif was also shown to stabilize the native conformation of the Tendamistat active sequence. Serine only in position *i* effects the geometry of the adjacent β-turn geometry; without the Bzl protecting group, the additional main chain−side chain hydrogen bond can be formed. As shown below, serine in other positions, as well as any protecting groups on Lys, Orn, or Arg, does not influence peptide conformations; in those cases, it is possible to use NMR data from peptides with protecting groups on Ser and Xaa (= Lys, Orn, Arg) and predict conformations of unprotected peptides.

For these peptides, turn structures are in agreement with all NOE-derived constraints and homo- and heteronuclear *J* coupling constants. The analysis of intense $C{=}O^{i+1} - C_\alpha H^{i+2}$ cross peaks in the H,C-COLOC or HMBC spectrum (only possible for ϕ angles between $-30°$ and $-90°$) additionally confirms the observed βII-turns in C1 and C2. Corresponding tables are given as supplementary material. The backbone dihedral angles averaged over the time span of the MD simulations are close to ideal values for each turn structure; there is no evidence for a conformational equilibrium of the peptide backbone in MD simulations.

The Tyr[6] side chain χ_1 angles for all peptides are predominantly in the $+180°$ orientation (ca. 40% in C1 and C3, 60% in C2 and C2e), while the Ser[3] side chain does not show a predominant conformation because either the diastereotopic $C_\beta H$ protons are overlapped or an equal distribution of all three rotamers is observed. Signal overlap also prevents analysis of the Trp[4] side chain for all peptides.

4.2. Cyclo(-D-Pro[1]-Ser[2]-Trp[3]-Xaa[4]-Tyr[5]-Ala[6]-) (C4, C5, and C6). The three peptides C4 (Xaa = Lys(Z); including Ser(Bzl)), C5 (Xaa = Orn(Z); including Ser(Bzl)), and C6 (Xaa = Arg(NO_2); no Ser protecting group) show similar conformations with *all-trans* peptide bonds deduced from MD simulations. Ser[2] is always located in position $i + 2$ of a β-turn; no structural influence on turn geometries is observed. The resulting structure of peptide C4 after averaging over different 60 ps MD simulations *in vacuo* is shown in Figure 3, while similar structures for C5 (averaging over different 60 ps MD simulations *in vacuo*) and C6 (averaging over different 80 ps MD simulations in DMSO solution) are presented in the supplementary material (Figure S1).

The Tyr[5] and Trp[3] side chain χ_1 angles adopt predominantly the $-60°$ orientation (ca. 70% each for C4, C5, and C6, respectively), while for Ser[2], no side chain conformations can be studied due to signal overlap.

All three peptides reveal the same pattern of two intramolecular hydrogen bonds from Ala_6NH to Trp[3]C=O and from Trp[3]NH to Ala[6]C=O, forming two connected β-turns. As expected from related peptides including D-proline, a βII′-turn was found to exist with D-Pro_1 and Ala_2 in positions $i + 1$ and $i + 2$, respectively, closed by a strong hydrogen bond involving the Trp[3] amide proton. This βII′-turn structure is in agreement with all NOE-derived constraints and homo- and heteronuclear *J* coupling constants.

However, the other region of these peptides shows no single backbone conformation, which fulfills all experimental data. Significant distance violations occur in this second β-turn with Xaa[4] ($i + 1$) and Tyr[5] ($i + 2$). Experimental data were found to be inconsistent unless multiple fast interconverting backbone conformers are taken into account.[34,35] A better description of NMR observables is possible by averaging[36] over conformational ensembles with at least two major backbone conformations using MD simulations with time-dependent distance constraints (MD^{tNOE}).[32] There have been a number of other approaches recently published to solve this problem in the structure refinement from NMR data.[37]

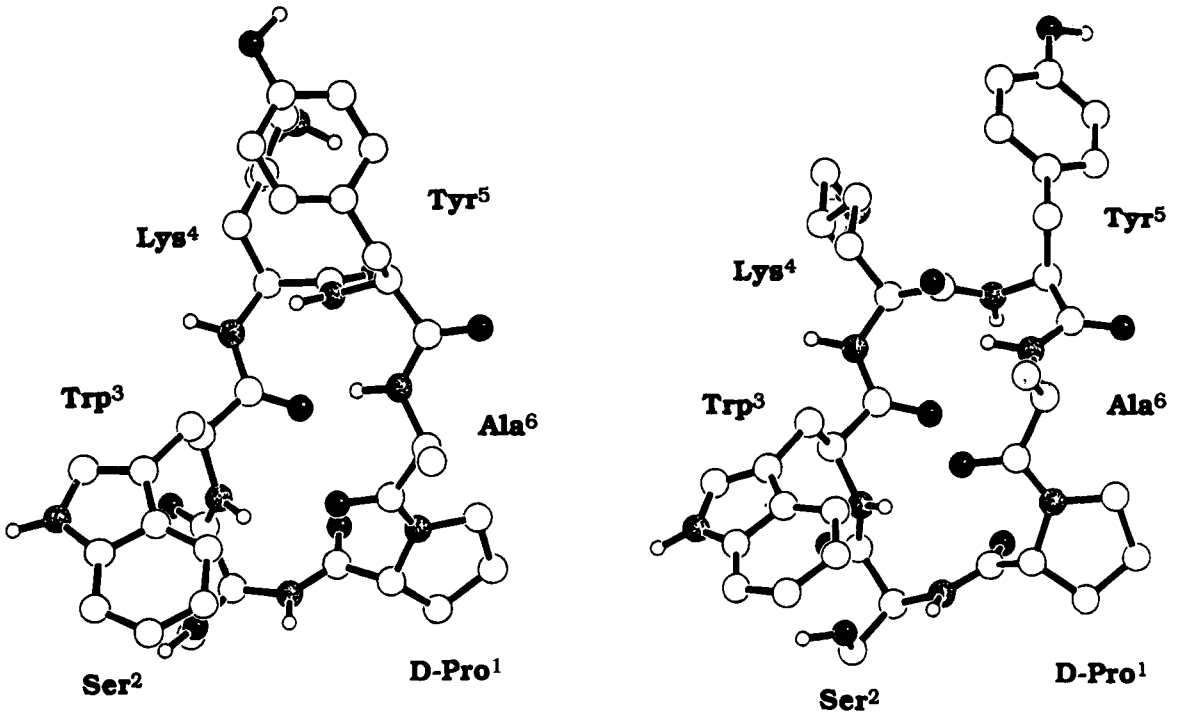

Figure 3. Averaged structures for cyclo(-D-Pro[1]-Ser[2](Bzl)-Trp[3]-Lys[4](Z)-Tyr[5]-Ala[6]-) (C4) each from 60 ps restrained MD *in vacuo*: (left) βII′/βI-backbone conformation and (right) βII′/βII-backbone conformation. No experimental information is available for the side chain conformations of Ser[2] and Lys[4]. Protecting groups and nonlabile hydrogens are not displayed.

Table 1. Selected Interproton Distances (pm) in Comparison with Distances for Ideal Type-I and Type-II Turn Geometries for Cyclo(-D-Pro[1]-Ser[2](Bzl)-Trp[3]-Lys[4](Z)-Tyr[5]-Ala[6]-) (C4)

protons		NOESY (DMSO)	ROESY (DMSO)	ROESY (MeOH)	βI-turn	βII-turn
Tyr[5]NH	Lys[4]C_αH	235	253	245	340−360	200−220
Tyr[5]NH	Tyr[5]C_αH	243	258	236	280−300	210−230
Tyr[5]NH	Tyr[5]$C_\beta H^{pro\text{-}S}$	317		300	340−360[a]	380−400
Tyr[5]N*H*	Tyr[5]$C_\beta H^{pro\text{-}R}$	264		267	240−260[a]	340−360
Tyr[5]NH	Ala[6]NH	254	280		290−320	260−290

[a] Calculated for $\chi_1 = -60°$ for the residue in position $i + 2$.

This situation is described in detail for C4 (cf. Tables 1−3). Here seven distance constraints (20% of the data set) involving Tyr[5]N*H* are analyzed in detail: the NOEs Tyr[5]N*H*−Tyr[5]$C_\alpha H$ (243 pm) and Tyr[5]N*H*−Lys[4]$C_\alpha H$ (235 pm) are slightly larger than those observed for ideal type-II turn geometries. This trend alone, which is observed for the "flexible" peptides C4−C9 with one D- and five L-amino acids, is not significant to postulate alternate backbone conformations. But five other NOEs can only be fulfilled by a βI-turn geometry: Tyr[5]N*H*−Tyr[5]$C_\beta H^{pro\text{-}R}$, Tyr[5]N*H*−Tyr[5]$C_\beta H^{pro\text{-}S}$, Tyr[5]N*H*−Trp[3]$C_\beta H^{pro\text{-}R}$, Tyr[5]N*H*−Ala[6]N*H*, and Tyr[5]N*H*−Lys[4]$C_\beta H$. All seven conflicting NOEs can only be fulfilled by taking fast interconverting backbone conformers (e.g., βII′/βII and βII′/βI) into account. Further complication of this situation is expected due to averaging effects from other than the two "ideal" β-turn geometries. The analysis of homonuclear $^3J(NH,C_\alpha H)$ and heteronuclear $^3J(NH,C_\beta)$ coupling constants (extracted from HETLOC spectra[38]) cannot solve this conflicting situation due to the ambiguity of the corresponding Karplus equations (Table 2). In combination both coupling constants are in agreement with two different φ angles for Tyr[5] (−91°/−98° for βI or 66°/58° for βII). Using $^3J(C_\alpha H,C{=}O^{i-1})$ heteronuclear coupling constants a discrimination is possible: The observed intense crosspeak between Lys[4]C=O and Tyr[5]C_αH in the HMBCS-270 spectrum is only in agreement with a βII-turn geometry (Tyr[5] $\phi = 80°$ in $i + 2$ position). However, without quantification, turn flexibility cannot be excluded.

The different βII′/βI or βII′/βII backbone geometries for C4−C9 are maintained in MD simulations *in vacuo* or in DMSO (for C6 and C9). No conformational changes occur with or without application of distance constraints, but strong NOE violations are observed in the postulated flexible turn region (for seven NOEs involving Tyr[5]N*H*). These violations are obvious in numerical analyses of constraint violations (Table 3 and supplementary material) or in simulations of theoretical 2D-NOESY spectra for both backbone conformers.[39] Both backbone conformers for C4 are presented in Figure 3. Simple

(34) (a) Kessler, H.; Bats, J. W.; Lautz, J.; Müller, A. *Liebigs Ann. Chem.* **1989**, 913−928. (b) Kessler, H.; Griesinger, C.; Lautz, J.; Müller, A.; van Gunsteren, W. F.; Berendsen, H. J. C. *J. Am. Chem. Soc.* **1988**, *110*, 3393−3396. (c) Stradley, S. J.; Rizo, J.; Bruch, M. D.; Stroup, A. N.; Gierasch, L. M. *Biopolymers* **1990**, *29*, 263−287. (d) Rowan, R., III; Warshel, A.; Sykes, B. D.; Karplus, M. *Biochemistry* **1974**, *13*, 970−981. (e) Kopple, K. D.; Bean, J. W.; Bhandary, K. K.; Briand, J.; D'Ambrosio, C. A.; Peishoff, C. E. *Biopolymers* **1993**, *33*, 1093−1099. (f) Bean, J. W.; Kopple, K. D.; Peishoff, C. E. *J. Am. Chem. Soc.* **1992**, *114*, 5328−5334. (g) de Leeuw, F. A. A. M.; Altona, C.; Kessler, H.; Bermel, W.; Friedrich, A.; Krack, G.; Hull, W. E. *J. Am. Chem. Soc.* **1983**, *105*, 2237−2246. (h) Scarsdale, J. N.; Yu, R. K.; Prestegard, J. H. *J. Am. Chem. Soc.* **1986**, *108*, 6778−6784. (i) Kim, Y.; Ohlrogge, J. B.; Prestegard, J. H. *Biochem. Pharmacol.* **1991**, *40*, 7−13. (j) Kopple, K. D.; Baures, P. W.; Bean, J. W.; D'Ambrosio, C. A.; Huges, J. L.; Peishoff, C. E.; Eggleston, D. S. *J. Am. Chem. Soc.* **1992**, *114*, 9615−9623. (k) Perczel, A.; Hollosi, M.; Sandor, P.; Fasman, G. D. *Int. J. Pept. Protein Res.* **1993**, *41*, 223−236.

(35) (a) Kessler, H.; Matter, H.; Gemmecker, G.; Kling, A.; Kottenhahn, M. *J. Am. Chem. Soc.* **1991**, *113*, 7550−7563. (b) Mierke, D. F.; Kurz, M.; Kessler, H. *J. Am. Chem. Soc* **1994**, *116*, 1042−1049. (c) Kessler, H.; Geyer, A.; Matter, H.; Köck, M. *Int. J. Pept. Protein Res.* **1992**, *40*, 25−40.

(36) Jardetzky, O. *Biochim. Biophys. Acta* **1980**, *621*, 227−232.

(37) (a) Brüschweiler, R.; Blackledge, M.; Ernst, R. R. *J. Biomol. NMR* **1991**, *1*, 3−11. (b) Landis, C.; Allured, V. S. *J. Am. Chem. Soc.* **1991**, *113*, 9493−9499. (c) Yang, J.; Havel, T. F. *J. Biomol. NMR* **1993**, *3*, 355−360. (d) Kenmink, J.; van Mierlo, C. P. M.; Scheek, R. M.; Creighton, T. E. *J. Mol. Biol.* **1993**, *230*, 312−322. (e) Bonvin, A. M. J. J.; Rullmann, J. A. C.; Lamerichs, R. M. J. N.; Boelens, R.; Kaptein, R. *Proteins: Struct. Funct. Genet.* **1993**, *15*, 385−400. (f) Torda, A. E.; Brunne, R. M.; Huber, T.; Kessler, H.; van Gunsteren, W. F. *J. Biomol. NMR* **1993**, *3*, 55−66.

(38) (a) Kurz, M.; Schmieder, P.; Kessler, H. *Angew. Chem., Int. Ed. Engl.* **1991**, *30*, 1329−1331. (b) Schmieder, P.; Kurz, M.; Kessler, H. *J. Biomol. NMR* **1991**, *1*, 403−420. (c) Schmieder, P.; Kessler, H. *Biopolymers* **1992**, *32*, 435−440.

(39) (a) Keepers, J. W.; James, T. L. *J. Magn. Reson.* **1984**, *57*, 404−426. (b) Program *Backcalculation* written by S. Seip, Ph.D. Thesis, Technical University Munich 1991.

Table 2. (Top) $^3J(NH,C_\alpha H)$ Coupling Constants (Hz) for Cyclo(-D-Pro[1]-Ser[2](Bzl)-Trp[3]-Lys[4](Z)-Tyr[5]-Ala[6]-) (C4), Cyclo(-D-Pro[1]-Ser[2](Bzl)-Trp[3]-Orn[4](Z)-Tyr[5]-Ala[6]-) (C5), and Cyclo(-D-Pro[1]-Ser[2]-Trp[3]-Arg[4](NO_2)-Tyr[5]-Ala[6]-) (C6) and Calculated Backbone Torsions[a] and (Bottom) $^3J(C_\alpha H,C_\beta H)$ Coupling Constants (Hz) and Calculated Populations of Side Chain Dihedrals for C4, C5, and C6

C4	Ser[2](Bzl)	Trp[3]	Lys[4](Z)	Tyr[5]	Ala[6]
$^3J_{NH,\alpha}$[b]	8.4	9.5	3.6	7.9	6.1
ϕ_{exp}[c]	−145	−134	−176	−149	−161
	−95	−106	−64	−91	−79
			108	66	89
			12	54	31
$^3J_{NH,C\beta}$[d]	1.0	1.4	1.5	1.5	1.6
ϕ_{exp}[c]	−171	−177	−178	−178	−179
	−107	−100	−98	−98	−96
	−13	−20	−22	−22	−24
	51	57	58	58	59
C5	Ser[2](Bzl)	Trp[3]	Orn[4](Z)	Tyr[5]	Ala[6]
$^3J_{NH,\alpha}$[b]	8.3	9.8	3.8	7.8	6.1
ϕ_{exp}[c]	−144	−134	−176	−149	−161
	−96	−106	−65	−91	−79
			107	67	89
			13	53	31
C6	Ser[2]	Trp[3]	Arg[4](NO_2)	Tyr[5]	Ala[6]
$^3J_{NH,\alpha}$[b]	8.0	8.5	4.7	8.5	7.0
ϕ_{exp}[c]	−148	−144	−169	−144	−155
	−92	−96	−71	−96	−85
			100		80
			20		40

	$^3J(H_\alpha,H_\beta{}^R)$[e]	$^3J(H_\alpha,H_\beta{}^S)$[e]	$\chi_1 = -60°$ (%)	$\chi_1 = 180°$ (%)	$\chi_1 = 60°$ (%)
C4					
Trp[3]	10.8	4.2	74	15	11
Tyr[5]	10.3	4.6	70	18	12
C5					
Trp[3]	10.8	4.0	74	13	13
Tyr[5]	10.3	4.6	68	11	21
C6					
Trp[3]	10.6	3.9	73	12	16
Tyr[5]	10.7	3.9	73	12	15

[a] Heteronuclear $^3J(NH,C_\beta)$ coupling constants and calculated backbone torsions are given for C4 only. [b] Experimental value from 1D spectrum (DMSO-d_6, 300 K). [c] Possible values for torsion ϕ (deg) via Karplus' equation. [d] Extracted from 500 MHz HETLOC. [e] Extracted from 250 MHz E. COSY.

averaging over both trajectories under the assumption of equally populated conformations ($p(\beta I) = p(\beta II) = 0.5$) shows for all peptides that the violated distance constraints are now in better agreement with experimental data.

The analysis of MD simulations with time-dependent distance constraints ($\tau = 2.5$ ps) reveals increased internal flexibility in the upper part of the cyclic peptide backbone. Experimental data are much better fulfilled by taking multiple interconverting backbone conformers into account, produced during the 90 ps time span of this *in vacuo* simulation. The two major conformers agree with the $\beta II'/\beta II$ and $\beta II'/\beta I$ backbone models. Figure 4 illustrates the observed flexibility for three important distance constraints in the upper region of C4 (Tyr[5]N*H*−Tyr[5]C$_\alpha$*H* (left), Tyr[5]N*H*−Lys[4]C$_\alpha$*H* (middle), and Tyr[5]N*H*−Tyr[5]C$_\beta$*H*$^{pro\text{-}R}$ (right); time-averaged distances used to calculate the penalty energy contribution (above) and actual distances in each conformer (below)). The calculated and time-averaged interproton distances show better agreement with the experiment using this modified sampling technique, especially for NOEs involving Tyr[5]N*H*. The physical nature for the large coupled distance variations as displayed in Figure 4 is due to the reorientation of the central Lys[4]−Tyr[5] amide bond to form two different β-turn structures. Better agreement with experimental data is also observed for $^3J(NH,C_\alpha H)$ coupling constants calculated as statistical averages over different conformations (no data given).

Table 3. Comparison between Experimental and Calculated Interproton Distances (pm) for Cyclo(-D-Pro[1]-Ser[2](Bzl)-Trp[3]-Lys[4](Z)-Tyr[5]-Ala[6]-) (C4)[a]

protons		NOESY	MD$^{\beta 1}$	MD$^{\beta 2}$	MD^{av}	MD^{tNOE}
Ser[2]NH	Ser[2]C$_\alpha$H	285	286	289	287	287
Ser[2]NH	Ser[2]C$_\beta$H	251[b]	291	292	291	294
Ser[2]NH	D-Pro[1]C$_\alpha$H	208	207	208	207	212
Ser[2]NH	D-Pro[1]C$_\beta$H	361[b]	372	367	370	367
Ser[2]NH	Trp[3]NH	239[d]	273	270	271	280
Ser[2]C$_\alpha$H	Ser[2]C$_\beta$H	234[b]	215	210	212	221
Trp[3]NH	Ser[2]C$_\beta$H	301[b]	383	396	389	364
Trp[3]NH	Ser[2]C$_\alpha$H	314	343	341	342	337
Trp[3]NH	D-Pro[1]C$_\alpha$H	336	370	359	364	386
Trp[3]NH	Trp[3]C$_\alpha$H	280	283	283	283	280
Trp[3]NH	Trp[3]C$_\beta$H$^{pro\text{-}R}$	246	246	249	248	276
Trp[3]NH	Trp[3]C$_\beta$H$^{pro\text{-}S}$	325	352	352	352	334
Trp[3]C$_\alpha$H	Trp[3]C$_\beta$H$^{pro\text{-}R}$	274	289	289	289	273
Trp[3]C$_\alpha$H	Trp[3]C$_\beta$H$^{pro\text{-}S}$	249	239	238	238	245
Tyr[5]NH	Tyr[5]C$_\beta$H$^{pro\text{-}S}$	317	350	409	379	348
Tyr[5]NH	Tyr[5]C$_\beta$H$^{pro\text{-}R}$	264	244	362	303	288
Tyr[5]NH	Trp[3]C$_\beta$H$^{pro\text{-}R}$	384	344	548	446	440
Tyr[5]NH	Lys[4]C$_\alpha$H	235	345	225	285	310
Tyr[5]NH	Tyr[5]C$_\alpha$H	243	279	211	245	268
Tyr[5]NH	Lys[4]C$_\beta$H	329[b]	318	415	367	389
Tyr[5]C$_\alpha$H	Tyr[5]C$_\beta$H$^{pro\text{-}R}$	298	288	283	285	272
Tyr[5]C$_\alpha$H	Tyr[5]C$_\beta$H$^{pro\text{-}S}$	249	244	247	245	251
Lys[4]NH	Lys[5]C$_\alpha$H	256	258	264	261	251
Lys[4]NH	Trp[3]C$_\alpha$H	229	242	254	248	247
Lys[4]NH	Trp[3]C$_\beta$H$^{pro\text{-}S}$	231	249	236	242	303
Lys[4]NH	Trp[3]C$_\beta$H$^{pro\text{-}R}$	296	349	329	339	347
Lys[4]NH	Lys[4]C$_\beta$H	275[b]	238	257	247	304
Lys[4]NH	Lys[4]C$_\gamma$H	323[b]	441	404	423	342
Lys[4]C$_\alpha$H	Lys[4]C$_\beta$H	273[b]	255	257	256	247
Lys[4]C$_\alpha$H	Lys[4]C$_\gamma$H	358[b]	328	309	319	331
Lys[4]N$_\epsilon$H	Lys[4]C$_\epsilon$H	249	238	245	242	241
Ala[6]NH	Tyr[5]C$_\beta$H$^{pro\text{-}S}$	352	398	374	386	373
Ala[6]NH	Tyr[5]C$_\beta$H$^{pro\text{-}R}$	308	321	315	318	350
Ala[6]NH	Tyr[5]C$_\alpha$H	293	332	341	337	319
Ala[6]NH	Ala[6]C$_\alpha$H	281	274	285	279	271
Ala[6]NH	Ala[6]C$_\beta$H	294[c]	332	299	315	321
Ala[6]NH	Tyr[5]NH	254[d]	240	310	275	275
Ala[6]NH	Trp[3]NH	317[d]	398	439	419	443
Ala[6]C$_\alpha$H	D-Pro[1]C$_\delta$H	207[c]	220	218	219	226
Ala[6]C$_\alpha$H	Ala[6]C$_\beta$H	252[c]	240	240	240	239

[a] Experimental data are extracted from a 600 MHz NOESY spectrum (DMSO-d_6, 300 K, 100 ms τ_{mix}). MD$^{\beta 1}$: 60 ps *in vacuo* with βI-turn. MD$^{\beta 2}$: 60 ps in vacuo with βII-turn. MD^{av}: averaging over both trajectories. MD^{tNOE}: 90 ps MD with time-dependent distance constraints. [b] 90 pm pseudoatom correction for upper bounds. [c] 100 pm pseudoatom correction for lower bounds. [d] 100 pm added for NH−NH distances to upper bounds to correct for chemical exchange.

Similar results due to improved sampling features were obtained from analyzing 90 ps MD^{tNOE} trajectories for peptides C5−C9. Corresponding tables are given in the supplementary material.

Further experimental data (line broadening effects in ^{1}H-NMR at lower temperatures (250−300 K) in methanol-d_3[40] and $T_{1\varrho}$ measurements (see below)) also support this model to explain conflicting NMR results.

4.3. Cyclo(-D-Pro[1]-Ser[2]-Trp[3]-Xaa[4]-Tyr[5]-Ser[6]-) (C7, C8, and C9). The three peptides C7 (Xaa = Lys(Z); including Ser$_2$(Bzl)), C8 (Xaa = Orn(Z); including Ser[2](Bzl) and Ser[6](Bzl)), and C9 (Xaa = Arg(NO_2); no Ser protecting group) show identical conformational preferences compared to the corresponding Ala[6]-containing peptides C4, C5, and C6. The substitution of Ala[6] versus Ser[6] was done to include an additional functional group adjacent to the active sequence of Tendamistat (Ser[21]) in the target cyclic peptides. The resulting structures for peptides C7 and C8 after averaging over different 60 ps MD simulations *in vacuo* are given in the supplementary material (Figure S2), while structures for C9 after averaging over different 80 ps MD simulations in DMSO solution are

(40) Matter, H. Ph.D. Thesis, Technical University Munich, 1992.

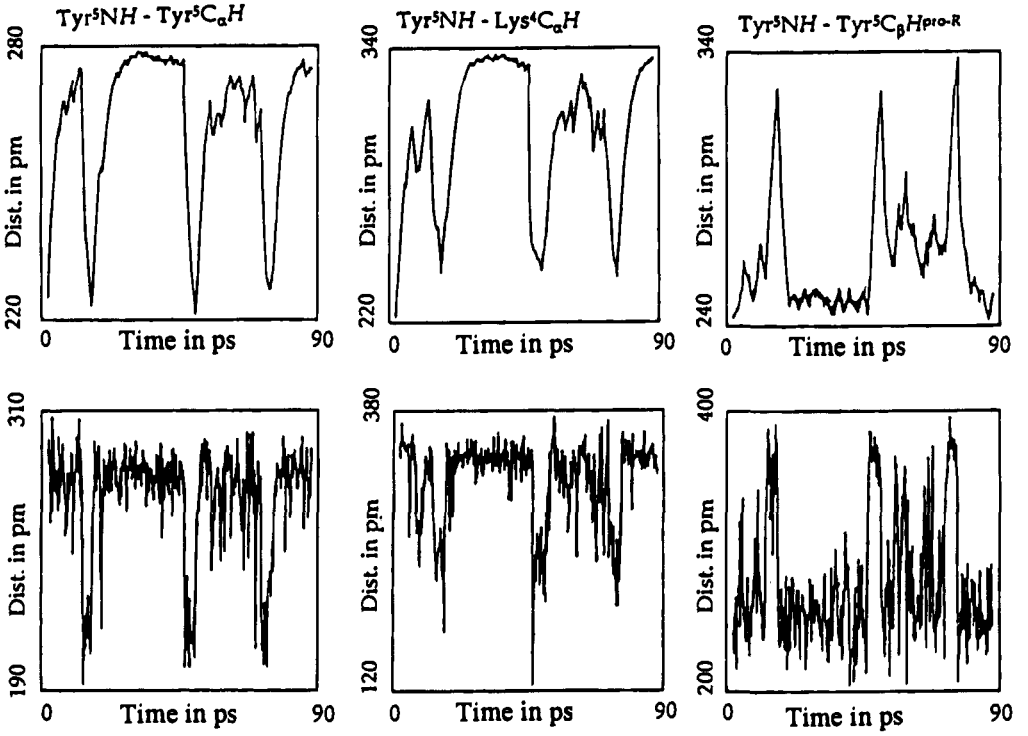

Figure 4. Results of the MD simulations with time-dependent distance constraints (MD^{tNOE}) for C4 cyclo(-D-Pro[1]-Ser[2](Bzl)-Trp[3]-Lys[4](Z)-Tyr[5]-Ala[6]-): time dependence of the NOE-derived distances $Tyr^5NH-Tyr^5C_\alpha H$ (left), $Tyr^5NH-Lys^4C_\alpha H$ (middle), and $Tyr^5NH-Tyr^5C_\beta H^{pro\text{-}R}$ (right) from the 90 ps MD^{tNOE} trajectory with $\tau = 2.5$ ps ((above) averaged "distance term" r' to calculate penalty energies[32] and (below) actual distance r).

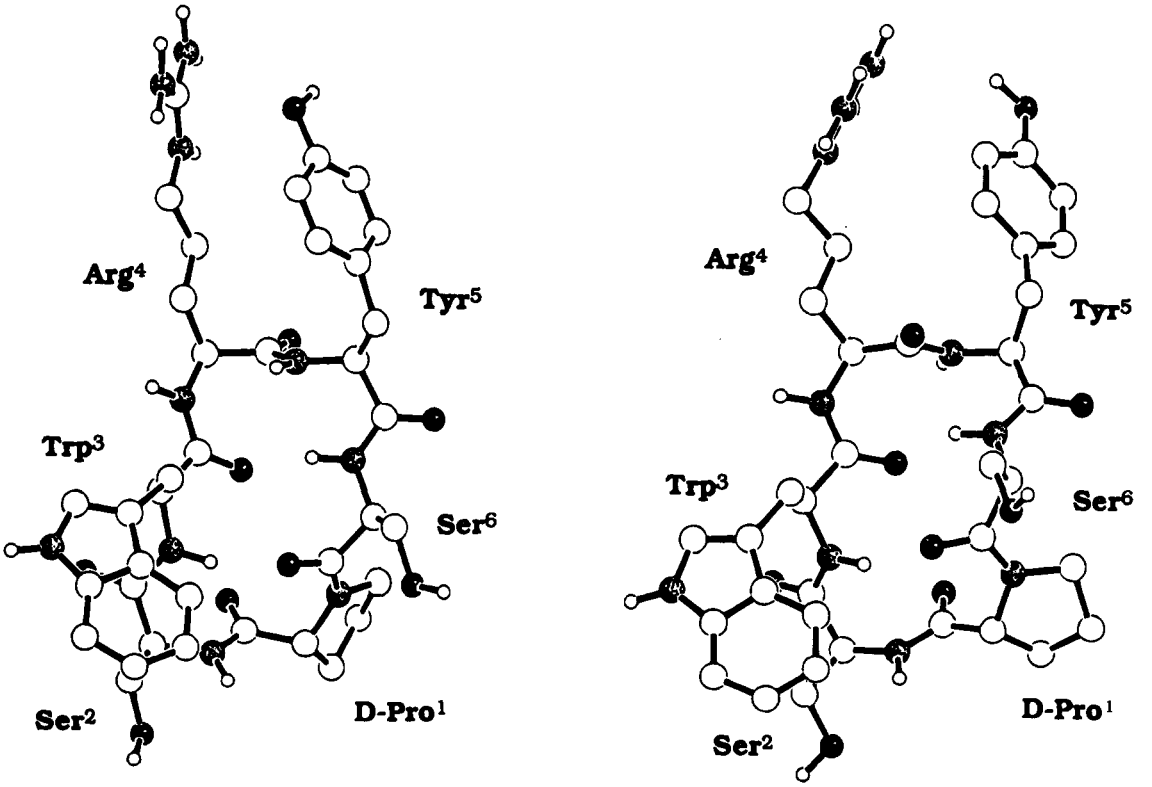

Figure 5. Averaged structures for cyclo(-D-Pro[1]-Ser[2]-Trp[3]-Arg[4](NO_2)-Tyr[5]-Ser[6]-) (C9) each from 80 ps restrained MD in DMSO: (left) βII′/βI-backbone conformer and (right) βII′/βII-backbone conformer. No experimental information is available for the side chain conformations of Ser_2 and Arg[4]. Protecting groups and nonlabile hydrogens are not displayed.

shown in Figure 5. The same hydrogen bond pattern from Ala_6-NH to $Trp^3C{=}O$ and from Trp^3NH to $Ala^6C{=}O$ forms two connected β-turns: a rigid βII′-turn (D-Pro[1] and Ser^2) and a very flexible reverse turn, showing a βI/βII equilibrium, again determined by analyzing the pattern of characteristic NOEs and coupling constants. Similar computational procedures to obtain averaging of all NMR observables were used to confirm this model of internal dynamics. In addition the measurement of relaxation rations $R_{1\varrho}$ for C7 provides further evidence for this dynamical model.

Again the Tyr^5 and Trp^3 side chain χ_1 angles adopt predominantly the −60° orientation (ca. 70% each for C7, C8, and C9,

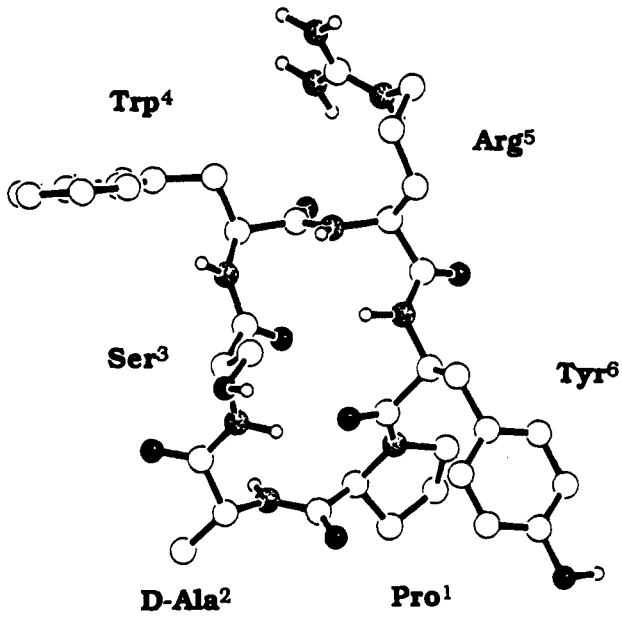

Figure 6. Averaged structure of cyclo(-Pro[1]-D-Ala[2]-Ser[3]-Trp[4]-Arg[5](NO$_2$)-Tyr[6]-) (C12) from a 80 ps restrained MD trajectory in DMSO at 300 K. No experimental information is available for the side chain conformations of Ser[3], Trp[4], and Arg[5]. Protecting groups and nonlabile protons are not displayed.

respectively), while for Ser[2], no side chain conformations can be studied due to signal overlap. The Ser[6] side chain mainly adopt the 180° orientation for C8 and C9 (ca 50% each), while for C7, no data can be obtained.

4.4. Cyclo(-Pro[1]-D-Ala[2]-Ser[3]-Trp[4]-Xaa[5]-Tyr[6]-) (C10, C11, and C12). The three peptides C10 (Xaa = Lys(Z)), C11 (Xaa = Orn(Z)), and C12 (Xaa = Arg(NO$_2$)), all without a Ser[3] protecting group, reveal similar conformations in solution. They were designed to study the influence of the bridging dipeptide sequence Pro$_1$-D-Ala$_2$ on the structure and dynamics of the Tendamistat-derived tetrapeptide sequence.

For C10 and C11 there are experimental indications for a *cis* orientation of the Tyr[6]−Pro[1] peptide bond in a minor populated isomer.[41,42] Both peptides show a second set of resonances in the ^{1}H-NMR spectra. Positive ROESY peaks confirm exchange between the two isomers; the *cis*-peptide bond is supported by the finding of a strong NOE signal between Tyr[6]C$_\alpha$*H* and Pro[1]C$_\alpha$*H* for both minor conformations (C10 and C11). Due to the low amount of these minor conformations in the equilibrium at 300 K, no attempts were made to elucidate more conformational details. For C12 only a single conformation with a *trans* orientation of this corresponding peptide bond was identified.

The resulting structure for C12 after averaging over 80 ps MD simulations in DMSO solution is shown in Figure 6. Similar structures for the major isomers of peptides C10 and C11 after averaging over 60 ps MD simulations *in vacuo* are given in the supplementary material. Pro[1] and Ala[2] adopt the positions $i + 1$ and $i + 2$ of a βII-turn in all peptides. The other moiety can be characterized by a slightly distorted βI-turn encompassing Trp[4] ($i + 1$) and Xaa[5] ($i + 2$). The theoretical ϕ angle for Trp[4] in an ideal βI-turn is −60°, while the combined analysis of ^3J(NH,C$_\alpha$H) and ^3J(NH,C$_\beta$) coupling constants reveals an angle pair of −89°/−93° for this fragment, which corresponds to the resulting torsion angles from MD simulations. All MD structures are in accord with all experimental data (NOEs, homo- and heteronuclear coupling constants ^3J(NH,C$_\alpha$H), ^3J(NH,C$_\beta$), and ^3J(C=O,C$_\alpha$H)). Both turn structures were closed by transannular hydrogen bonds in DMSO solution, as proposed by NMR measurements and confirmed in MD simulations.

A side chain conformational analysis shows that the Tyr[6] side chain χ_1 angles adopt predominantly the −180° orientation, while for Ser[2], no side chain conformations can be deduced due to signal overlap. It is remarkable that as for C2e and C3 the location of the hydroxy amino acid serine influences the turn geometry in the adjacent β-turn: the Xaa[5]NH in the central Trp[4]−Xaa[5] amide bond is forced to direct into the same hemisphere as the L-amino acid side chains (corresponding to a βI-turn).[33] However it should be mentioned that due to the signal degeneracy of the Ser[3]C$_\beta$*H* protons the MD simulations do not provide evidence for a stabilizing side chain−main chain hydrogen bond involving Ser[3]O$_\gamma$. Here no attempts were made to simulate models with other preformed Ser[3] χ_1 angle distributions.

4.5. Cyclo(-D-Ala[1]-Pro[2]-Ser[3]-Trp[4]-Xaa[5]-Tyr[6]-) (C13, C14, and C15). The three peptides C13 (Xaa = Lys(Z); including Ser$_3$(Bzl)), C14 (Xaa = Orn(Z); including Ser(Bzl)), and C15 (Xaa = Arg(NO$_2$)) contain a Ser residue in position *i* of a β-turn; its influence on turn conformation is not neglectible. Using this backbone template, the influence of the bridging dipeptide sequence D-Ala[1]-Pro[2] on the structure and dynamics of the Tendamistat active sequence was studied.

For the Ser[3]-protected peptides C13 and C14, similar conformations were found to exist in solution. The resulting structures for C13 after averaging over different 60 ps MD simulations *in vacuo* and for C15 after averaging over different 80 ps MD simulations in DMSO solution are shown in Figure 7. For C14, structures after averaging over 60 ps MS simulations *in vacuo* are given in the supplementary material (Figure S4).

Again two transannular hydrogen bonds (Ser[3]NH- - -Tyr[6]C=O and Tyr[6]NH- - -Ser[3]C=O) form a typical hexapeptide motif. D-Ala[1] and Pro[2] adopt the $i + 1$ and $i + 2$ positions of a βII′-turn, confirmed by NOEs and the small ^3J(NH,C$_\alpha$*H*) coupling constant for D-Ala[1], which is in agreement with a 60°−75° ϕ torsion angle. The unusual position of Pro[2] in the $i + 2$ position of a reverse turn can be explained by a stronger directing effect of the D-amino acid in the *i* position of a βII′-turn.

All experimental data count for internal mobility in the other moiety of these peptides. Similar methods (MD^{tNOE} simulations and averaging over two different backbone conformers βII′/βI and βII′/βII) were used to obtain an ensemble of conformations, which better fits all experimental data. However, the analysis of MD simulations with time-dependent distance constraints reveals more backbone dihedrals with increase mobility, counting for more complicated dynamical phenomena, which cannot be described in detail by only two main conformers. Therefore the substitution of D-Pro against a noncyclic D-amino acid (D-Ala[1]) leads to increased backbone flexibility in cyclic hexapeptides.

While for C15 again a βII′-turn is observed for D-Ala[1]-Pro[2], its other moiety can be characterized by a βI-turn encompassing Trp[4] and Arg[5]. This conformational change can be explained with the position of Ser[3] (in position *i* of a β-turn; without protection group only for C15). Additionally, the Arg[5]N$_\alpha$*H* temperature gradient suggests the contribution of this proton to an additional hydrogen bond. Furthermore for Ser[3] the side chain rotamer with a χ_1 dihedral of 60° is found to exist

(41) Kessler, H.; Anders, U.; Schudok, M. *J. Am. Chem. Soc.* **1990**, *112*, 5908−5916.

(42) (a) Mierke, D. F.; Yamazaki, T.; Said-Nejad, O. E.; Felder, E. R.; Goodman, M. *J. Am. Chem. Soc.* **1989**, *111*, 6847−6849. (b) Bairaktari, E.; Mierke, D. F.; Mammi, S.; Peggion, E. *J. Am. Chem. Soc.* **1990**, *112*, 5383. (c) Deber, C. M.; Madison, V.; Blout, E. R. *Acc. Chem. Res.* **1976**, *9*, 106−112. (d) Siemion, I. Z.; Wieland, T.; Pook, K. H. *Angew. Chem., Int. Ed. Engl.* **1975**, *14*, 702−705.

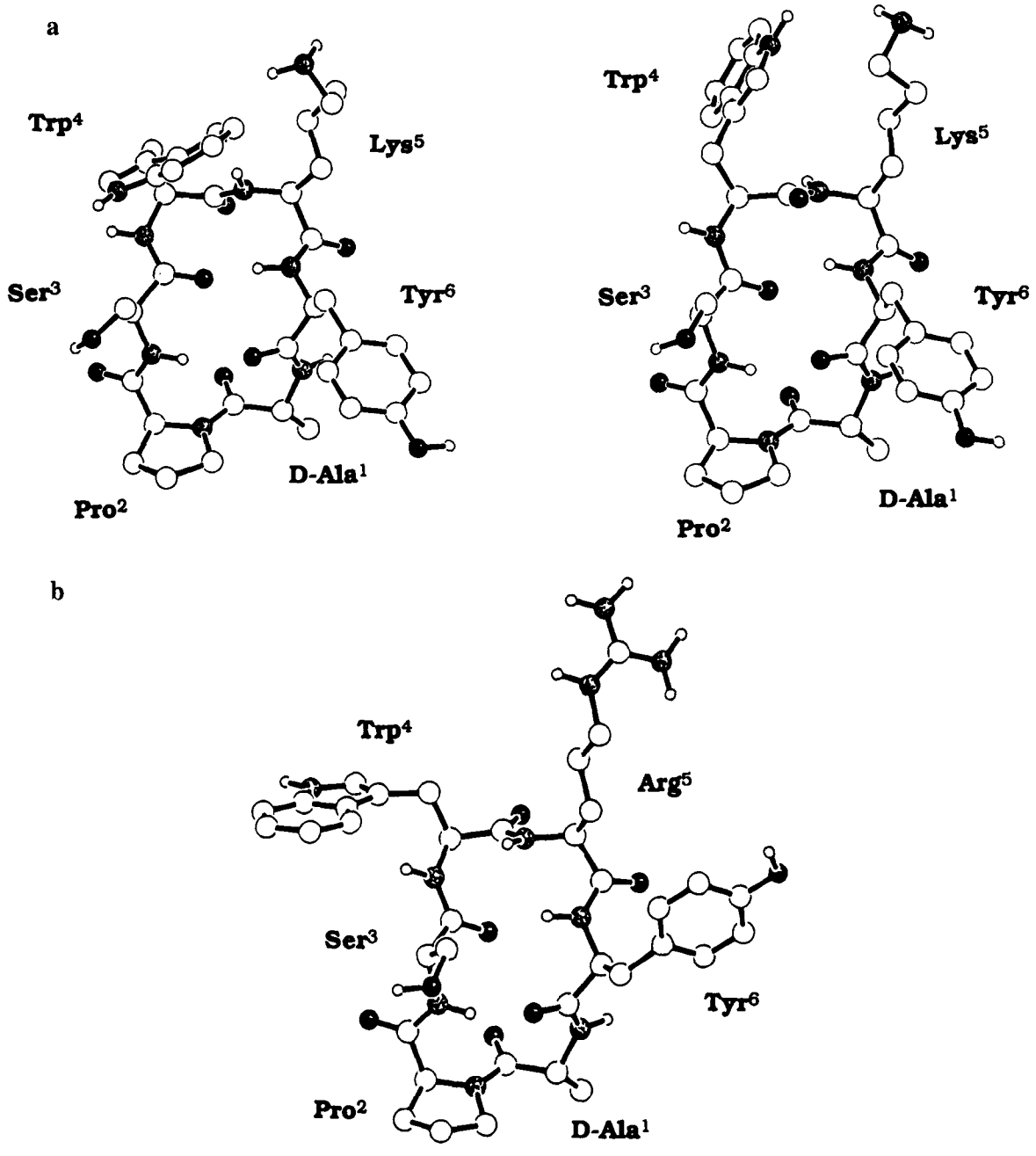

Figure 7. (a) Averaged structures of cyclo(-D-Ala[1]-Pro[2]-Ser[3](Bzl)-Trp[4]-Lys[5](*Z*)-Tyr[6]-) (C13) from each 60 ps restrained MD *in vacuo*: (left) βII′/βI-backbone conformer and (right) βII′/βII-backbone conformer. No experimental information is available for the side chain conformations of Ser[3], Trp[4], and Lys[5]. (b) Averaged structure of cyclo(-D-Ala[1]-Pro[2]-Ser[3]-Trp[4]-Arg[5](NO$_2$)-Tyr[6]-) (C15) from a 80 ps restrained MD simulation in DMSO. No experimental information is available for the side chain conformations of Trp[4] and Arg[5]. Protecting groups and nonlabile hydrogens are not displayed.

predominantly in solution (56% from coupling constant analysis). However, this additional hydrogen bond is not observed during the MD trajectories either *in vacuo* or in DMSO solution for C15 due to improper sampling of Ser side chain conformations. No different side chain starting conformations for Ser[3] or additional torsion constraints were used for further simulations. It can be concluded from these comparisons that serine in position *i* of a β-turn stabilizes the type-*I* geometry from an equilibrium of multiple interconverting turn conformations.

4.6. Relaxation Studies. To examine the internal mobility for βI/βII turn conformations, rotating frame relaxation studies ($T_{1\varrho}$ relaxation times)[27] were measured for backbone amide protons of C2, C4, C7, C10, and C13 (one member of each peptide family) at three different spin-lock fields B_1 at 500 MHz (Table 4). Conformational exchange becomes observable up to $<10^{-5}$ s^{-1}.[43] The conformational exchange contribution $R_{1\varrho}$(exch) to the relaxation rate $R_{1\varrho} = 1/T_{1\varrho}$ depends on the exchange rate between different conformers and the square of the chemical shift differences.[44] These will be maximal when the exchange occurs at a rate near the frequency corresponding to the spin-lock field B_1 (between 1 and 10 kHz).

The contributions of $R_{1\varrho}$ relaxation rates are significantly larger than the R_1 relaxation rates for each amide proton. These $R_{1\varrho}$ rates can be described as

(43) Brüschweiler, R.; Roux, B.; Blackledge, M.; Griesinger, C.; Karplus, M.; Ernst, R. R. *J. Am. Chem. Soc.* **1992**, *114*, 2289–2302.

(44) (a) Deverell, C.; Morgan, R. E.; Strange, J. H. *Mol. Phys.* **1970**, *18*, 553–559. (b) Strange, J. H.; Morgan, R. E. *J. Phys. Chem.* **1970**, *74*, 1999–2011. (c) Bleich, H. E.; Glasel, J. A. *Biopolymers* **1978**, *17*, 2445–2457.

$$R_{1\varrho}(\text{obs}) = R_{1\varrho}(\text{dd}, {}^{1}\text{H}) + R_{1\varrho}(\text{dd}, {}^{14}\text{N}) + R_{1\varrho}(\text{sr}) + R_{1\varrho}(\text{exch}) \quad (1)$$

$R_{1\varrho}$(obs) is the measured relaxation rate, $R_{1\varrho}$(dd, ^{1}H) and $R_{1\varrho}$(dd, ^{14}N) are the amide proton rotating frame dipolar relaxation rates for neighboring protons and nitrogen, and $R_{1\varrho}$(sr) reflects scalar relaxation, the modulation of NH coupling by ^{14}N relaxation. The chemical exchange contribution $R_{1\varrho}$(exch) is calculated for each NH (Table 4) as described previously.[45] From ^{13}C T_1 measurements of C4[46] a rotational correlation time τ_c of 0.4 ns was calculated and used for determination of the $R_{1\varrho}$(dd, ^{1}H) by calculation of the ratio $R_{1\varrho}$(dd, ^{1}H)/R_1(dd, ^{1}H) for all related peptides.[27]

The differences in the mobilities of various amide protons from $R_{1\varrho}$ and $R_{1\varrho}$(exch) rates can be correlated with results from MD simulations (cf. ref 33 for C2 and C2e). For C7 the amide protons of Tyr^5(i + 2) and Ser^6(i + 3) reveal the largest $R_{1\varrho}$(exch) contribution, counting for increased mobility of the flexible βI/βII-turn and the corresponding hydrogen bond Ser$_6$-NH- - -Trp^{3}C=O. In contrast, the opposite βII′-turn and the corresponding hydrogen bond donor Trp^{3}NH are more rigid. Reduced mobility of amide protons as hydrogen bond donors is found in MD simulations and relaxation studies, although different time scales are the basis of these complementary techniques. However there is no clear correlation of the $R_{1\varrho}$(exch) rate with N*H* chemical shift temperature gradients. The contribution of the chemical exchange is dependent on the field strength of the spin lock only for the flexible amide protons in C7. All other amide protons show no clear correlation, which can be explained by contributions of higher frequent mobilities.

The interpretation of the relaxation measurements for C4 again shows correspondence to the results from the MD simulations: the amide protons of Tyr^5 and Ala^6, both found in the flexible β-turn, again have higher $R_{1\varrho}$(exch) rates than all other amide protons. Ser^{2}NH as central amide proton in the rigid βII′-turn also has slighly increased $R_{1\varrho}$(exch) rates because this proton is not involved in a hydrogen bond. However the $R_{1\varrho}$(exch) rate is much higher for Tyr^{5}NH as the central amide proton in the opposite flexible turn. At higher temperatures (310 and 320 K), the differences in the $R_{1\varrho}$(exch) rates for different amide protons disappear. The increased temperature reduces the effective lifetime of the conformational substates involved in the dynamical interconversion. Hence, this conformational interconversion cannot be monitored by $T_{1\varrho}$ measurements at increased temperatures, while the analysis of 2D-NOESY and ROESY spectra at 310 and 320 K still reveals the presence of the conflicting NOE-derived distances.[40]

Unfortunately, this *two-site* model is too simplistic for conformational exchange in peptides of any complexity. But it can be assumed that internal mobility involving motions of larger amplitudes correlate with larger differences for chemical shifts, which will be reflected in increased $T_{1\varrho}$ contributions. Due to the absence of a more specific model for any dynamical process within each of these peptides, a more detailed interpretation of these data is prevented. However, the model presented here is consistent with experimental data and theoretical simulations indicating rigid and flexible turns within cyclic peptides.

The $R_{1\varrho}$(exch) rates measured for C10 are relative high, counting for intramolecular mobility. The peptide backbone is not as rigid as deduced only from analysis of NOE effects, coupling constants, and MD simulations. However, the data do not support any model of dynamical interconversions in

(45) Kopple, K. D.; Bhandary, K. K.; Kartha, G.; Wang, Y. S.; Parameswaran, K. N. *J. Am. Chem. Soc.* **1986**, *108*, 4637–4642.
(46) Balbach, J.; Matter, H.; Kessler, H. Unpublished results.

Table 4. Proton Relaxation Rates (s^{-1}) in Labor Frame (R_1) and Rotating Frame ($R_{1\varrho} = 1/T_{1\varrho}$) for C4, C7, C10, and C13[a]

C4

	Ser^{2}NH	Trp^{3}NH	Lys^{4}NH	Tyr^{5}NH	Ala^{6}NH
300 K					
R_1	1.3	1.1	1.5	1.4	0.9
$R_{1\varrho}$(dd)	2.0	1.8	2.4	2.3	1.4
$R_{1\varrho}$					
10.8 kHz	10.8	7.9	10.3	13.6	14.5
6.8 kHz	12.0	9.3	11.8	16.1	16.9
4.5 kHz	12.0	9.9	12.8	16.9	18.8
$R_{1\varrho}$(exch)					
10.8 kHz	7.8	5.2	6.9	10.4	12.2
6.8 kHz	9.0	6.6	8.4	12.9	14.6
4.5 kHz	9.8	7.2	9.4	13.8	16.5
310 K					
R_1	1.7	1.5	2.1	1.9	1.1
$R_{1\varrho}$(dd)	2.8	2.3	3.3	3.0	1.8
$R_{1\varrho}$					
10.8 kHz	8.6	6.5	8.7	9.9	9.3
6.8 kHz	9.2	6.5	9.1	10.0	9.5
4.5 kHz	9.2	6.7	9.2	10.5	10.5
$R_{1\varrho}$(exch)					
10.8 kHz	5.8	3.2	4.4	6.0	6.6
6.8 kHz	6.4	3.2	4.7	6.1	6.8
4.5 kHz	6.4	3.4	4.8	6.6	7.8
320 K					
R_1	1.7	1.5	2.1	1.8	1.2
$R_{1\varrho}$(dd)	2.8	2.5	3.4	2.9	1.9
$R_{1\varrho}$					
10.8 kHz	6.6	5.1	7.0	6.4	6.2
6.8 kHz	7.0	5.5	7.5	6.9	6.8
4.5 kHz	7.6	6.1	8.1	*b*	7.8
$R_{1\varrho}$(exch)					
10.8 kHz	2.9	1.7	2.6	2.5	3.3
6.8 kHz	3.3	2.1	3.1	3.0	3.9
4.5 kHz	3.9	2.7	3.7		4.9

C7

	Ser^{2}NH	Trp^{3}NH	Lys^{4}NH	Tyr^{5}NH	Ser^{6}NH
R_1	1.0	0.8	1.3	1.1	0.8
$R_{1\varrho}$(dd)	1.6	1.2	2.1	1.8	1.3
$R_{1\varrho}$					
10.8 kHz	18.5	8.8	13.2	22.2	20.0
6.8 kHz	18.2	9.3	13.3	23.2	22.2
4.5 kHz	17.8	9.4	13.3	23.8	23.2
$R_{1\varrho}$(exch)					
10.8 kHz	16.0	6.6	10.2	19.5	17.8
6.8 kHz	15.7	7.1	10.2	20.5	20.0
4.5 kHz	15.3	7.2	10.3	21.1	21.0

C10

	D-Ala^{2}NH	Ser^{3}NH	Trp^{4}NH	Lys^{5}NH
R_1	1.4	0.9	1.4	1.5
$R_{1\varrho}$(dd)	2.2	1.5	2.2	2.4
$R_{1\varrho}$				
10.8 kHz	14.9	21.7	17.5	14.3
6.8 kHz	16.4	22.2	17.8	14.7
4.5 kHz	18.2	23.2	18.8	14.9
$R_{1\varrho}$(exch)				
10.8 kHz	11.8	19.3	14.3	10.9
6.8 kHz	13.3	19.8	14.6	11.3
4.5 kHz	15.1	20.8	15.6	11.5

C13

	D-Ala^{1}NH	Ser^{3}NH	Trp^{4}NH	Lys^{5}NH
R_1	1.0	0.7	1.3	1.6
$R_{1\varrho}$(dd)	1.6	1.1	2.1	2.5
$R_{1\varrho}$				
10.8 kHz	23.8	22.2	10.1	15.2
6.8 kHz	24.4	21.3	10.6	16.3
4.5 kHz	24.4	26.3	11.4	16.9
$R_{1\varrho}$(exch)				
10.8 kHz	21.3	20.2	7.1	11.7
6.8 kHz	21.9	19.3	7.6	12.8
4.5 kHz	21.9	24.3	8.4	13.4

[a] Obtained at 300 K and 500 MHz (for C4 additional data at 310 and 320 K were measured). [b] No values due to signal overlap.

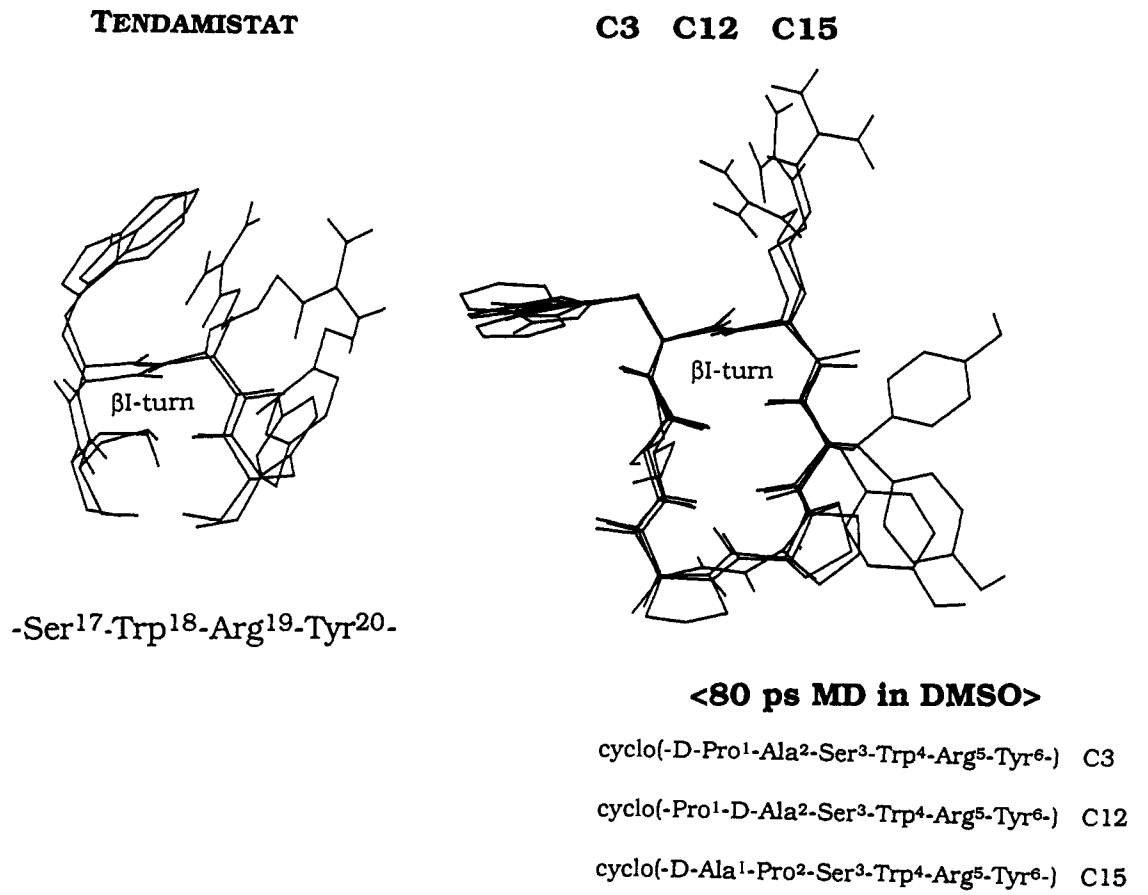

Figure 8. Structural comparison of the Tendamistat active sequence (left) in βI-turn conformation[6b] with three superimposed peptide conformations for C3, C12, and C15 (right). These three peptides show similar structural features (βI-turn for the tetrapeptide sequence) but use different bridging amino acids to constrain the sequence of interest. Due to the lack of experimental data, it was not possible to determine preferences for the Trp^4 and Arg^5 side chain χ_1 dihedrals. The displayed side chain conformations were obtained from analysis of MD simulations.

β-turns. All hydrogen bonds tend to be less stable than in the other peptides with D-proline in position *i* of a βII′-turn. This structural element has a stabilizing influence on cyclic hexapeptides, while the βII-turn with L-Pro^1 and D-Ala^2 in C10 induces more flexibility.

Relatively large contributions of the $R_{1\varrho}$(exch) rates were measured for C13. The values for D-Ala^1NH and Ser^3NH in the βII′-turn are larger than for Trp^4NH and Lys^5NH within the postulated flexible region, showing the increased mobility in βII′-turns without stabilizing effects by conformationally directing residues like D-proline. The postulated internal flexibility in the upper β-turn based on NOE data cannot be confirmed by these measurements. The large value for Ser^3-NH as the hydrogen donor reveals the instability of the corresponding hydrogen bond. This observation additionally corresponds to the relatively large temperature gradient for this amide proton (−4.9 ppb/K), which could not be explained on the basis of the model derived from MD simulations alone. The measured contributions of chemical exchange to the $R_{1\varrho}$ rates cannot be correlated with a simple conformational model, as it is possible for all other peptides (C2, C2e, C4, C7, and C10).

5. Discussion

5.1. Peptide Structures. All hexapeptides contain only one D-amino acid, but they can be classified in different backbone families. Conformational control using the appropriate peptide backbone templates allows rebuilding of the native βI-turn conformation of the Tendamistat active sequence (e.g., in C1e, C2e, C3, C10, C11, C12, and C15). In other peptides the triad Trp^{18}-Arg^{19}-Tyr^{20} is now arranged in a "shifted" turn arrangement: these key amino acids adopt the "wrong" positions within the standard turn conformation. The substitution of Arg against Orn or Lys does not affect the overall conformation of the peptide backbone. D-Proline has the strongest conformational directing effect: in all those peptides rigid βII′-turns with D-Pro in position *i* + 1 closed by a strong hydrogen bond are found. The other moiety with two L-amino acids shows either a βI-turn, a βII-turn, or a flexible structure with both turn types in fast conformational equilibrium. Serine (or threonine) in position *i* of these *all*-L-turn structures stabilize the type-I turn. This important effect can now be used for further peptide design.[33]

With L-Pro and a D-amino acid in a cyclic hexapeptide, the relative position of both residues determines the corresponding turn types: for Pro-D-Ala (C10−C12), a βII-turn is found with Pro in position *i* + 1, while for D-Ala-Pro (C13−C15), a βII′-turn can be identified. As displayed in Figure 8, the backbone conformations of peptides C3, C12, and C15 are in perfect agreement with the native βI-turn conformation of Ser^{17}-Trp^{18}-Arg^{19}-Tyr^{20} found in Tendamistat. Thus it is possible to rebuild conformational features in smaller peptides and to control the conformation of a given peptide sequence.

5.2. Biological Activity. The geometrical match for some of the aforementioned peptides (e.g., C3, C12, and C15) to Tendamistat leads to small but significant biological activity as α-amylase inhibitors. All 15 protected and unprotected peptides (C1e = C1 deprotected) were tested by following the procedures described in refs 1, 2, and 10. The K_I values for the arginine-containing peptides are between 120 and 277 μM, for all other peptides between 96 and >3000 μM, while for Tendamistat, a K_I value of 2×10^{-10} M can be measured. The deprotected peptides with the highest biological activity as

porcine pancreas α-amylase inhibitors are C3e (120 μM (K_I value)), C4e (99 μM), C6e (260 μM), C9e (199 μM), C13e (153 μM), C14e (96 μM), and C15e (277 μM). All other peptides have K_I values higher than 500 μM. For the homolog series of peptides C1e (1800 μM), C2e (3100 μM), and C3e (120 μM), the influence of the basic amino acid on ligand binding is very pronounced: it could be shown that Arg[19] is a necessary prerequisite to improve biological activity, while for the ornitine or lysine analogs, the activity is reduced. Similar observations were made for C7e (579 μM), C8e (2100 μM), and C9e (199 μM), but for C10e, C11e, and C12e, no significant biological activity could be measured (each >2000 μM). However, it is interesting to note some exceptions here: for C13e (153 μM), C14e (96 μM), and C15e (277 μM), the ornitine-containing peptide is the most active one, while for C4e (99 μM), C5e (>1000 μM), and C6e (260 μM), the lysine-containing peptide shows significant biological activity. Within the series of arginine-containing peptides with the active triad Trp-Arg-Tyr in the native βI-turn conformation (C3e, C12, and C15), C3e with D-Pro and Ala in positions $i + 1$ and $i + 2$ of a "flat" and rigid βII′-turn geometry shows the highest biological activity, suggesting this particular structural motif within the "bridging region" as most compatible with structural requirements on the ligand binding process. The conformation of L-proline with the five-membered ring oriented perpendicular to the flat cyclic peptide backbone in positions $i + 1$ or $i + 2$ of standard β-turns might be responsible for lowering the biological activity in those cases. Furthermore, the position $i + 2$ seems to be more favorable than the $i + 1$ position for a steric bulky five-membered ring pointing to the same direction than all other L-amino acid side chains.

It should be mentioned here that in parallel studies[10] the peptide cyclo(-D-Pro-Phe-Ala-Trp-Arg-Tyr-) shows a K_I value of 14 μM, while for cyclo(-D-Pro-Phe-Ser-Trp-Arg-Tyr-), a K_I value of 32 was measured. The conformations of these compounds are related to C3e with D-Pro-Phe in the bridging region in a βII′-turn. It is remarkable that the replacement of Ala in C3e against Phe lead to a significant increase in the biological activity. For other cyclic peptides in this study, inhibition constants between 160 and 460 μM were measured. The corresponding linear hexapeptide precursors show activities between 320 and 670 μM, while various linear tripeptides (the active triad Trp-Arg-Tyr with different protection groups) reveal inhibition constants between 240 und 1100 μM. A remarkable exception here is the linear peptide Ac-Trp-Arg-Tyr-OMe (100 μM), which was shown to act as competitive inhibitor on amylase. The peptides based on the "wrong" rigid templates with the active triad exposed in a sheet-like conformation or a shifted-turn structure indeed show lower inhibition constants, while for C3e, the inhibition constant is in the same range as that for this linear tripeptide.

5.3. Conclusion. The inhibition constants for some of the cyclic peptides here show that the structural-based design using rigid peptide templates can be used to mimic the active loop from a macromolecule by small constrained peptides maintaining the key residues in the favored biologically active conformation. For some of the hexapeptides described above in our publication, the structural constraints do not allow the active triad to adopt the βI-turn observed in Tendamistat, which is reflected by lower biological activity. In addition, some of these peptides are also more active than linear precursors, demonstrating the effect of conformational constraints and the loss of internal mobility as entropic effects on ligand binding properties.

However all biological activities reported here and from Etzkorn et al.[10] are not as high as observed for Tendamistat itself, leading to the conclusion that many more surface residues of Tendamistat are involved in the strong binding to α-amylase, although only the four residues 17−20 are conserved in a series of similar amylase inhibitor proteins. This finding is confirmed by preliminary structural information from the high-resolution X-ray structure of the intermolecular 1:1 Tendamistat/α-amylase complex.[47] Here α-amylase complexed with Tendamistat undergoes considerable conformational changes from its free solid-state conformation (*induced fit*[48]). Moreover it is obvious that a larger region than only the tetrapeptide sequence Ser_{17}-Trp_{18}-Arg_{19}-Tyr_{20} at the top of the first loop of the amylase inhibitor is required for a high complex binding constant.

These peptides together with previously reported data for linear and cyclic peptides enable us to correlate specific structural elements (conformation of the active triad and of the bridging region, amino acids in this bridging region) with biological activity, thus leading to deeper insight into the process of amylase inhibition by small cyclic peptides. The fact that it was possible to capture a significant part of the biological activity for the protein Tendamistat using cyclic peptides as "small molecule" mimics is stimulating for further studies in this direction.

6. Experimental Section

Solid-phase peptide synthesis was done by following general synthetic methods, as described in ref 33 for C2. Details for the synthesis of all 15 cyclic hexapeptide and analytical data are given elsewhere.[40] Details describing the methods of the determination of the inhibitory effect of these peptides on porcine pancreas α-amylase are described elsewhere.[1,2,10]

NMR spectra were acquired on Bruker spectrometers: AMX 600, AMX 500, and AC 250. The samples contained between 5 and 15 mg of the cyclic peptides C1−C15 in 0.5 mL of DMSO-d_6 (99.9 % ^2H atoms; Aldrich). All chemical shifts are referenced to the DMSO-d_6 signal at 2.5 ppm for ^1H and 39.5 ppm for ^{13}C. All experiments were acquired as described before.[33,35a]

Acknowledgment. Financial support by the Deutsche Forschungsgemeinschaft and the Fonds der Chemischen Industrie is gratefully acknowledged. H.M. thanks the Fonds der Chemischen Industrie for a fellowship. The authors thank Dr. L. Vértesy, Dr. R. Bender (both Hoechst AG) and Prof. P. A. Bartlett and Dr. T. Guo (both UC Berkeley) for inhibition assays and biological testing; Dr. C. Zechel (BASF) for deprotection of three peptides; E. Lichte, M. Kranawetter, S. Glocker, and B. Bitto (TU München) for HPLC separations; and Dr. J. Winkler (TU München) for FAB−MS spectra. Furthermore, we thank Prof. P. A. Bartlett, Prof. R. Huber (MPI Martinsried), and Prof. J. Engels (University of Frankfurt) for making their preliminary results available.

Supplementary Material Available: An additional 30 tables and four figures with ^1H and ^{13}C chemical shifts for all 15 peptides, selected J coupling constants, comparisons between experimentally determined and simulated NOE-derived distances for all peptides except C4, and peptide structures from various MD simulations for C5, C6, C7, C8, C10, C11, and C14 (39 pages). This material is contained in many libraries on microfiche, immediately follows this article in the microfilm version of the journal, can be ordered from the ACS, and can be downloaded from the Internet; see any current masthead page for ordering information and Internet access instructions.

JA943663N

(47) Huber, R.; Epp, O.; Wiegand, G. Personal communication.
(48) Koshland, D. *Proc. Natl. Acad. Sci. U.S.A.* **1958**, *44*, 98−104.